CZECH TECHNICAL UNIVERSITY IN PRAGUE
FACULTY OF MECHANICAL ENGINEERING

BACHELOR THESIS

3D PRINTED FUEL GRAIN OF HYBRID ROCKET ENGINE

Prague, 2018

Author: Ivan Šonka

Declaration

I declare that I have developed and written this Bachelor thesis completely by myself, under guidance of thesis supervisor Mgr. Jaroslav Kousal, Ph.D. All sources used are declared in the list of literature.

……

Anotační list

Jméno autora:	Ivan Šonka	
Název BP:	3D tištěné zrno hybridního raketového motoru	
Anglický název:	3D printed fuel grain for hybrid rocket engine	
Akademický rok:	2017/2018	
Ústav:	Ústav letadlové techniky	
Vedoucí BP:	Mgr. Jaroslav Kousal Ph.D.	
Bibliografické údaje:	Počet stran:	73
	Počet obrázků:	27
	Počet tabulek:	51
	Počet příloh:	1 (na CD)
Klíčová slova:	Palivové zrno, 3D tisk, hybridní raketový motor	
Keywords:	Fuel grain, 3D print, hybrid rocket engine	

Anotace: Cílem této bakalářské práce je zjistit je-li možné použít 3D tištěné palivové zrno v malém hybridním raketovém motoru s N_2O jako okysličovadlem. Navrhnout zrno a zjistit tah a využití zrna. Připravit testovací exemplář a charakterizovat jej.

Abstract: Goal of this bachelor thesis is to find out if 3D printed plastic fuel grain can be used in small hybrid rocket engine with N_2O oxidizer. Design its internal structure and develop a rough model of thrust profile and grain utilization. Prepare a demonstrator of the grain and characterize it.

Acknowledgement

I would like to thank to Mgr. Jaroslav Kousal Ph.D. for his guidance and advice during my work on bachelor thesis. Also to Ing. Kučera and Ing. Tomáš Čenský Ph.D. for their assistance with design and construction of the measuring device and 3D printing.

My undying gratitude is also towards my family that has supported me not only throughout the work on bachelor thesis, but throughout whole university and my entire life.

Table of contents

I. Introduction

Rocket engines are categorized by phase state of their propellants. In hybrid engines there is usually oxidizer, substance that supplies oxygen needed for combustion, in liquid state and fuel in solid phase state. Engines using solid oxidizer and liquid fuel are still labelled as hybrid engines, though they are very uncommon, because of production difficulties.

Other two types, complex liquid and simplest solid are used more frequently. Most famous commercial use of hybrid engine is on the Virgin galactic's Space ship 1 and 2. Despite this, hybrids still hold some crucial advantages in comparison to both liquids and solids.

In recent years 3D printing industry is on the rise. Using 3D printers and CAD software almost everyone can design and manufacture various products. Most common 3D printers are affordable and the technology is based on layering thin stripes of molten plastic through the nozzle, until the final product is completed. Technology can vary and it is not only plastic that can be printed. Nowadays metal printing is also an option, but it is still very expensive and used for very specific parts, for example used in jet engines, because of highly precise manufacturing this method offers.

II. Theory

1. Background on hybrid engines

Essentially there are three types of rocket propellants liquid, solid and hybrid rocket engines. Liquid rockets, in which both oxidizer and fuel are liquid and kept separate, until mixed and ignited in the combustion chamber right before the nozzle. Second type is solid rocket engine. In the solid rocket, the oxidizer and fuel are mixed in a single solid mass and combustion occurs when the surface is exposed to a combustion flame and heated to the ignition temperature. Hybrid engines uses both solid and liquid as propellants. In the most commonly used hybrids the oxidizer is liquid and fuel is solid as seen in Fig 1.

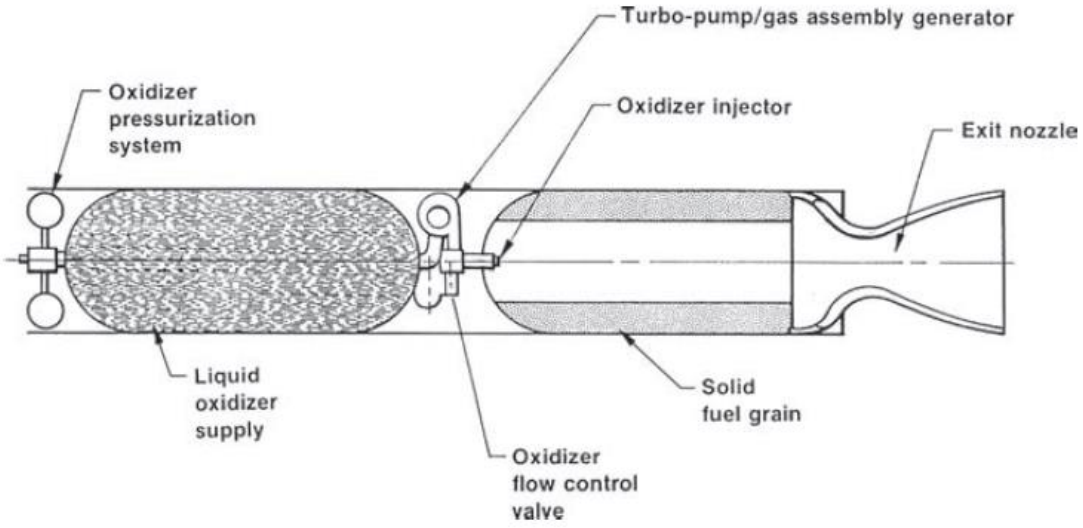

Fig. 1 Hybrid rocket engine schematics [1]

The hybrid rocket engines hold some key advantages over the other two types, making it highly desirable for academic groups, amateur rocket scientists and modellers.

- Safety: Unlike liquid engines, hybrid does not use toxic substances such as hydrazine and in comparison with solid, where the fuel and oxidizer are mixed in highly combustible substance, the fuel is inert and therefore there is no danger of explosion. Fuel grain cracks are also non-catastrophic since the burning only occurs in areas exposed to oxidizer.
- Low cost: Engine plumbing system is simpler and makes production cheaper. Fuel fabrication can be made in a commercial facility, which can be located near the launch

site and thus saving operational expenses. Whole system can also tolerate design margins, resulting in lower manufacturing costs.

- Simplified throttling: Hybrid can be throttled by managing oxidizer flow. In liquids one must synchronize flow of both the oxidizer and fuel and this can not be done at all by solid engines, since once these are ignited, there is no way of modulating the combustion or terminating the engine.

Of course there can not be advantages without experiencing some disadvantages.

- Low regression rate: Surface of the fuel grain needs to be exposed to the flame and oxidizer to burn efficiently. Therefore at larger grains need to require multiple ports to provide adequate burning surface. Unskilled grain design will also result in insufficient burning out of the fuel, with the remains of the grain becoming useless dead weight, that could have, with proper engineering, served for payload.
- O/F shift: Oxidizer/fuel weight ratio can shift during burning and lower the overall performance of the engine.
- Combustion efficiency: The nature of the large diffusion flame results in a lower degree of mixing and, hence, a lower impulse efficiency. This loss is generally greater than in solids or liquids.

2. History of hybrid rocketry

First attempts for usage of hybrid rocket engine surfaced in 1930s. In these times scientist in Germany, Soviet Union and USA recognized solid propellants as too volatile and dangerous, after some experiments that resulted in deaths. With solid engines out of the picture many of rocket engineers turned towards liquid or hybrid engines.

What is considered to be the first ever rocket launch propelled by hybrid engine happened on 17th august 1933. Flight was made by soviet rocket GIRD-09. Reached altitude was of 1500 meters, had a thrust of 500N and was flown for a time of 15s. This sounding rocket used gelled gasoline and LOX as propellants. In some sources this rocket is listed as liquid propelled but generally it is considered as first successful hybrid engine in use.

Soon after GIRD-09 Germany began with its own experiments using coal as solid and nitrous oxide as liquid, these attempts proved coal to be of little use as propellant for thrust provided by it was negligible. In the USA it was wood that was first used as solid and also as a material for the nozzle. Nozzle was quickly eliminated by the heat and wood was soon replaced by the aluminium alloy. Douglas fir, used as solid propellant, got replaced by wax loaded with carbon black and finally by rubber-based fuel, which was used in successful test, along with LOX as oxidizer.

In 1960s interest in hybrid rocketry rose and as a result many research projects were conducted. As a result, many various combinations of liquid and solid propellants were discovered.

3. Examples of typical fuels and oxidizers

Substances best performing as solid fuels are natural rubber and polymeric synthetic rubbers based on polybutadiene monomer (PB) with formula C_4H_6. "Typical polymers based on PB, PB-acrylonitrile (PBAN), PB-acrylic acid (PBAA), HTPB" (HTPB=hydroxyl-terminated PB) "and carbon-terminated PB (CTPB). The most popular of this group, based on cost and commercial availability is HTPB."[1] In smaller applications paraffin waxes, plexiglas, nylon and polyethylene are used. Various additives can be used to enhance I_{sp} or mechanical properties of the fuel. "A partial list of these additives include Al, AlH_3, Li, LiH, $LiAlH_3$, Li_3AlH_6, B, $B_{10}H_{14}$, $LiBH_4$ etc."[1]

Fuel grain material	**Oxidizer**	**I_{sp} [lbfs/lb]**	**I_{sp} [Ns/kg]**
HTBP	LOX	280	2745,86
HTBP	N_2O	247	2422,24
HTBP	N_2O_4	258	2530,12
HTBP	FLOX	314	3079,29
HTBP/40%Al	LOX	274	2687,02
HTBP/40%Al	N_2O	252	2471,28
HTBP/40%Al	N_2O_4	261	2559,54
HTBP/60%Al	FLOX	312	3059,68
Carbon	Air	184	1804,42
Carbon	LOX	249	2441,86
Carbon	FLOX	236	2314,37

Table 1: Example of specific impulse generated by some of the used oxidizer/fuel combinations [1]

Oxidizers used in hybrid and liquid rockets are essentially the same. In the forefront stands O_2 alongside FLOX (fluorine/LOX mixture) as most energetic. Other

suitable substances are N_2O_4, HNO_3, ClF_3, N_2O etc. N_2O is used in small modeller rocket engine on which all the tests have been conducted.

4. Fuel grain regression rate

Like other propulsion systems hybrid rocket engines use energy from combustion of fuel and oxidizer to generate thrust. However, as mentioned before, oxidizer and fuel are both stored separately and usually in different phases, in classical hybrids oxidizer is liquid and fuel grain solid. Oxidizer is injected in the head end of the fuel grain and mixes with the pyrolyzed gaseous fuel. This mixture then travels along the length of the fuel grain port, being the combustion chamber at the same time, and further reacts with solid fuel. Hot gasses produced during the reaction are blown out of the nozzle and thus generating thrust.

„The key parameter influencing the design of hybrid fuel grains, and, therefore, the overall hybrid-motor design, is the solid-fuel regression rate. The regression rate, a velocity, is defined as the rate at which the solid-phase fuel is converted to a gas.“[1] In different literature sometimes terms such as ablation rate, erosion rate or burning rate, being correctly used for depiction of burning inside solid fuel rocket engines, can be found. Unlike with solid propellants, where combustion appears on the surface of the fuel, at hybrid engines combustion rather happens at a boundary layer above the fuel surface. In order for this to happen fuel grain must first undergo either sublimation, phase transition from a solid to gas without entering liquid phase, or pyrolysis. This term refers to solid-gas phase change due to temperature accompanied by a chemical change,” such as the polymer chain breaking, cyclization, and re-organization that occurs in the in-depth near-surface region when polymer-based fuels degrade and regress.”[1] For example solid cryogens, such as frozen methane, sublime, while paraffin waxes tend to pyrolyze.

Proper fuel grain design is essential for getting desired specific impulse in a similar way as choosing which combination of oxidizer and grain material. Wrong design of the combustion ports, in fact fuel grain cross section, results in lower specific impulse, or incomplete burning of the grain, therefore having useless weight in rocket, that could have been used for payload. Internal ballistics of the hybrid engine are set by the fuel regression rate.

Moments after ignition and injection of the oxidizer reacting boundary layer is formed above the fuel grain surface. This boundary layer is commonly assumed to be turbulent, thanks to high Reynolds number of the injected oxidizer, but laminar and transition flow regimes may also appear at certain areas of the grain, turbulent flow is thought to be dominant cause of mass, momentum and energy exchange.

"Shortly after ignition, a diffusion flame region forms in the boundary layer. … the flame resides at a location approximately 10–20% of the boundary-layer thickness above the surface. Heat from the flame is convected and radiated to the fuel surface. This energy flux causes the solid fuel to pyrolyze (undergo a physical change accompanied by chemical changes). The pyrolyzed fuel vapor is then transported to the flame zone by convection and diffusion, where it mixes with the gaseous oxidizer, which has been transported through the boundary layer from the core flow region via turbulent diffusion. The two components react in the diffusion flame, a process that provides heat to sustain further fuel pyrolysis. The fuel mass flux due to pyrolysis, however, blocks some of the heat transfer to the surface, which causes a decrease in the regression rate and corresponding strength of the wall blowing effect and, in turn, a weakening of the blocking action, which in turns means that more heat can reach the surface, and so on. This tendency toward a self-regulating interaction between heat flux, mass blowing, and heat flux blockage is a distinguishing characteristic of hybrid combustion."[1]

Boundary layer is split into several layers normal to the grain surface. Below the flame exits fuel rich layer and above flame oxidizer rich layer, as can be seen on the Fig. 2, gaseous oxidizer may pass through the flame and start reacting with pyrolyzing fuel surface.

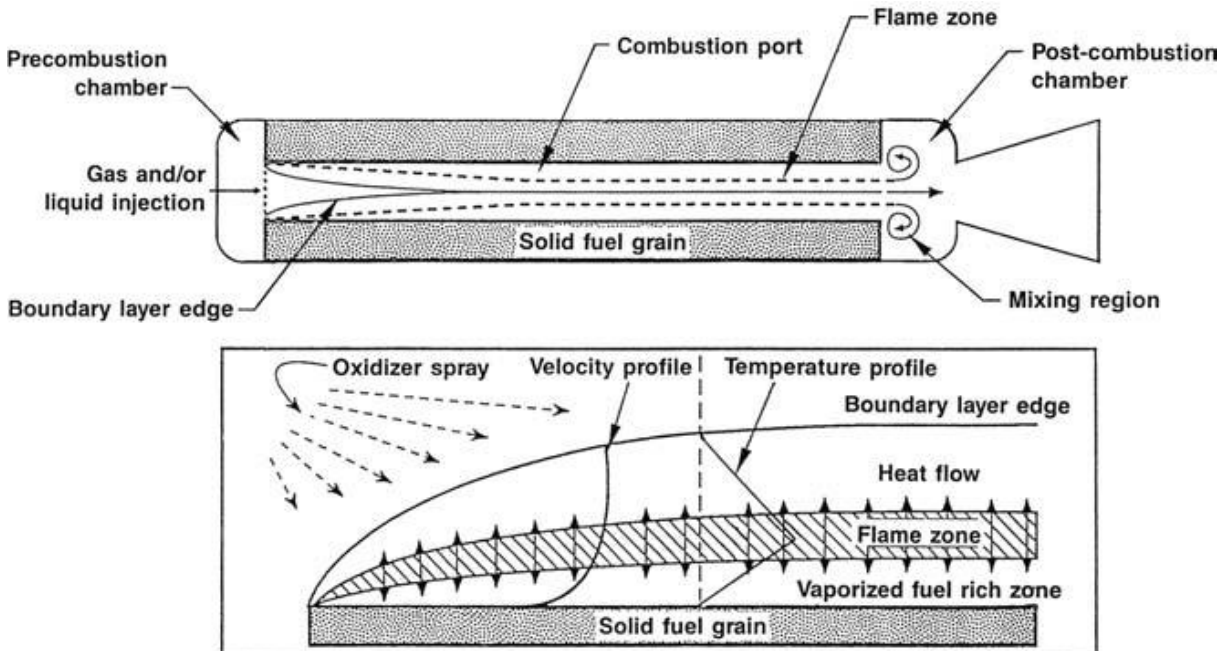

Fig. 2 Combustion layers schematics [1]

Based on heat transfer, combustion can be described by following equation:

$$Q_{tot} = \rho_f r \left[\left(\sum_i^n Y_i + \Delta H_{f,i}^O \right) - \Delta H_{f,HTPB}^O \right] + \rho_f r \sum_i^n Y_i + \left[\int_{T_{ref}}^{T_s} c_{p,i} dT \right]$$

Eq. (1) Heat flux during combustion [1]

Q_{tot} represents total hear transfer between the surface and boundary layer, ρ_f stands for fuel density, r is the regression rate, Y_i mass fraction, ΔH_f^O heat of formation of the fuel, c_p specific heat, T_s means surface temperature and T_{ref} reference temperature, usually 298K for which heat of formation can be found in chemical tables. Eq. (1) is simplified and is taking in account heat transfer via conduction, enthalpy leaving the surface via regression process and due to the bulk motion and diffusion, while neglecting the heat flux from pyrolyzing surface because of thermal radiation from beneath the surface.

As for fuel grain design there are many parameters that can influence the combustion. Amongst the most important of course stands the overall grain shape design and design of the combustion port, and ports number. Surface roughness affect heat transfer, in combination with fuel grain additives, usually metal particles introduced to improve mechanical properties and/or to either increase or decrease overall bulk density of the grain, it modifies the ability of the grain to withstand exposure to extreme pressure

in the combustion port. On the other hand, undesired result of the adjustments may be, for example, creation of liquidized fuel layer on the grain surface, caused by insufficient heat flux to cause phase transition of the solid fuel. This layer causes heat blocking effect.

Gas flow during combustion, in all hybrid engines, is always happening between grain surfaces, meaning the flow is similar to an internal pipe flow. Along the fuel grain length therefore may appear increase in flow velocity along the axial direction. Boundary layers may even grow to such extent, that they merge at certain areas.

Practical mass flux regime, that affects regression rate, is bound between two extremes, upper limit, called "flooding" limit, means that oxidizer mass flow is too high for the system to sustain combustion, by either extinguishing the flame or by making the fuel port too enriched with oxidizer, so it can no more sustain combustible reactions. Flooding limit depends of specific oxidizer/fuel combination and is higher for high energetic combinations. Lower limit, usually refered to as "cooking" limit, happens in situation when the mass flux is very low. This lowers the regression rate and heat transfers more slowly to the grain surface, taking longer time to pyrolyze and resulting in the heat wave penetrating deeper into the grain. Heat might cause, depending on the type of grain, melting, charring or depolymerisation reactions under the surface, all these cases have undesirable effects on the overall combustion efficiency and lowering reliability of the operation.

Regression rate behaviour has been object of many studies, various scientists has attempted, using various methods, to find the best way to describe mechanics behind this phenomenon. One of the earliest investigations was conducted by Bartel and Rannie and presented in Bartel H. R., and Rannie,W. D., "Solid Fuel Combustion as Applied to Ramjets,"[1],[9]. Their research was based on turbulent airstream entering carbon tube of known diameter *D* with known inlet velocity, pressure, density and total temperature. They made several assumptions such as fuel and air were completely mixed all along the tube. By examining the rate of heat added to the gas flowing through an elemental cross-sectional area, they obtained the following expression:

$$\rho_f r = \frac{1}{2} c_f G f_m exp\left(-2c_f x/D\right)$$

Eq. (2) Earliest expression describing regression rate [1]

On the left side of Eq. (2) is represented $\rho_f r$ the mass burning rate of fuel per unit area. On right side we have friction coefficient on the fuel surface c_f, average mass flux down the tube G, fuel/air ratio f_m, distance along the tube x and inner diameter D. According to this equation burning rate ought to decrease exponentially with axial position along the tube length.

Research on the boundary layer combustion was done by other scientist at the time, some of them assumed laminar flame zone in the boundary layer or done measurements by burning tubes of material and measure temperature during the reaction, stop the reaction, measure the fuel thickness and restart the test again. These start-ups and shutdowns may have caused error in the result. Together these experiments laid groundwork for future investigation done in this field.

Most influential theory on hybrid rocket engine combustion was introduced by Marxman and Gilbert in early 1960s. In their work they assume that flame splits boundary layer into two zones, one above and one below the flame. Upper zone, being oxidizer rich, has temperature and velocity gradients with opposite directions, lower zone, fuel rich, has gradients with same direction. "The flame occurs at a position where the concentrations of each are sufficient for combustion to occur" [1]. Assuming heat transfer from flame to grain surface as the controlling mechanism of the combustion they applied simplified energy flux balance and obtained following expression:

$$\rho_f r \Delta H_{v,eff} = Q_{tot}$$

Eq. (3) Regression rate based on simplified energy flux [1]

ρ_f stands for solid fuel density, r for regression rate, Q_{tot} for total heat transfer to the fuel surface per unit area, $\Delta H_{v,eff}$ represents total energy required to heat a unit mass of fuel from initial temperature to surface temperature and to vaporize it afterwards.

By further assuming turbulent flow in the boundary layer throughout the whole length of the fuel grain, analogy between Reynolds number and unity of Lewis and Prandtl numbers in the upper and lower boundary layer zones. Third assumption stated that velocity profile in the boundary layer is mostly unaffected by the combustion, in later endeavours in this field of study was proven that this effect can on the contrary have significant influence. Final equation describing solid fuel regression rate formed by these assumptions:

$$\rho_f r = CGRe_x^{-0,2}(St/St_O)\left(u_e/u_{fl}\right)\left[\left(h_{fl} - h_w\right) - \Delta H_{v,eff}\right]$$

Eq. (4) Heat flux during combustion [1]

"Where C is a function of the mainstream Mach number (about 0.03 for the low Mach numbers encountered in hybrids), G the local mass flux due to both oxidizer injection and all upstream fuel addition, St the Stanton number, St_O the Stanton number in the absence of blowing for turbulent flow over a flat plate, u_e the velocity at the edge of the boundary layer, u_{fl} the velocity at the flame, $h_{fl}$the stagnation enthalpy at the flame temperature, h_w the enthalpy at the wall in the gas phase, and $\Delta H_{v,eff}$ the total heat of gasification…" [1]

In years to come after presenting this research it was proven to be accurate for even for modern fuels. Many modifications for these early attempts were also presented, taking in account various other chemical and physical phenomenon affecting the combustion and regression rate, for example thermal radiation, variability of fluid and transport properties in the boundary layer, chemical kinetics, radiant heat transfer, injector and fuel additives effect etc. Number of scientists presented their own equations for regression rate, either correcting some of the assumptions made earlier or adding terms to describe certain effects that has been previously neglected.

Regression rate can also be described simply by equation:

$$r = \frac{dR(t)}{dt}$$

Eq. (5) Regression rate based on dimension change over time [2]

Knowing the fuel grains radius, for tube shaped grain, by measuring it at different times during the combustion, for example by shutting down and restarting the process, as mentioned before, and thus getting R(t). Regression rate is then simply calculated by time differentiation.

5. Basics of 3D print

5.1. Introduction

3D print technology is fairly new and still in development and is showing great promise. By 3D print we understand act of producing object based on its digital 3D model. "3D printing won't completely replace traditional manufacturing processes. Rather it will augment current means of mass production." [7] There is plenty of ways to do so and

different printing technologies shall be discussed later. 3D print evolved from technology of Rapid prototyping, and nowadays this term still can be used for 3D print. Rapid prototyping was used by companies to print out a prototype before mass production of the product, allowing to find flaws in construction, or the product in general and thus saving money. At this time Rapid prototyping was expensive technology, unavailable for wider use. In 1988 FDM technology, based on plastic extrusion, is developed and later in 1992 first printer using this technology introduced to market, making 3D printing affordable for wider public. “There are two main types of consumer 3D printers: those that use filament for fused deposition modelling (called FDM) and those that use resin for stereolithography (called SLA)” [7]

5.2. Technologies of 3D print

FFF (fused filament fabrication) also known as FDM (fused deposition modelling), patent protected term, is 3D printing process that uses continuous filament of thermoplastic material. Material is being fed from a coil, through moveable, heated extruder head. Material is melted and forced out of the printer nozzle. FFF technology produces final piece layer by layer, computer-controlled extruder head moves in 2 dimensions and after finishing each layer moving slightly upwards to begin new slice.

First part of the printing is creating CAD (computer aided design) model of the desired part, which is then processed by software and mathematically sliced in layers for the build. Most 3D printers support .STL files. CAM (computer aided manufacturing) software package controls the extrusion head and moves over the bed via set of servo or stepper motors. Material is melted in the heating chamber situated before nozzle and then extruded on the bed surface.

This technology the most popular for hobbyist-grade 3D printing. Other technologies may offer better results as for quality of the product, but the costs are incomparable. FFF machines can be acquired for less than $1000. Some of the parts can be manufactured by 3D printers, making repairing easier. Workplace dimensions usually are 30x30x60 cm, with machine price growing rapidly for bigger workplaces. More complex designs might need supports during the printing. Important properties of these printers are build volume, area in which the nozzle operates, materials which can be printed, layer resolution, thickness of the printed layer, lower resolution allows more detail print, build speed, stating how much of volume can be printed per second, and travel speed, max speed with which can the nozzle travel inside the workspace.

Among materials able to be used in such printers are mostly thermoplastics such as ABS, PLA, nylon, PET-G and will be discussed later. Every material requires different handling, because of differences in the glass transition temperature or thermal expansivity behaviour. For some heated printing bed must be used in order to avoid flaws caused by after print cooling.

SLA (stereolithography) is a form of 3D printing based on photopolymerization, process in which exposure to light causes molecules to form chains and forming polymers. Those then make up a solid 3 dimensional body. Almost any type of design can be made by this method, although it can be expensive to do so.

UV laser light is focused on photopolymer resin filled vat and with aid of CAM it is moved above the resin. Photosensitive polymers solidifies and forms a single layer of final object, similarly to FFF it forms the object layer by layer. SLA is used for rapid prototyping, SLA made products have sufficient mechanical properties to be machined. Other application for this technology is in medicine. Models of organs, bones etc. can be made using this method based on CT, MRI or other scans. Models can be used for preoperative planning, to aid diagnose or as implants prototypes.

Greatest disadvantage of SLA is price, SLA machines can cost hundreds of thousands of dollars and photosensitive resins can priced as high as thousand dollars per gallon.

SLS (selective laser sintering) is using laser to sinter, process of compacting material by heat or pressure without melting it to the point liquefaction. Materials typically used for this technology are nylon or polyamide. Laser is automatically pointed at points in space based on computer model and binds material into solid structure. It is similar to DMLS, which is discussed next.

High power laser is aimed at the surface powdered with desired material. Laser scans cross section, generated from CAD model, on the powder and fuses powder particles into solid layer. In next step powder bed moves one layer thickness lower and new layer of powder is applied. Laser scans new cross section, making second layer of final object and so on, until final product is completed.

Objects with complex geometry, impossible to produce using machining or any other additive technology, can be made using this method. Both prototypes and end products can be made this way very fast, while still having very good mechanical

properties. Disadvantage is that objects made by this method usually have porous surface, requiring some sort of finish or coating.

SLM (selective laser melting) also known as **DMLS** (direct metal laser sintering) as said above this method has many in common with SLS, biggest difference is the fact that SLM is melting the material, thus being able to change crystal structure, and usually works with metals.

Principles of SLM are generally the same as with SLS. SLM producing usually happens in atmosphere of inert gasses, either nitrogen or argon with low oxygen levels present. Layers worked are typically 20 micrometres.

Materials workable by this technology must exist in atomized form in order to be processed. Copper, titanium, gold and tungsten stand as examples of can be worked. Among alloys usable for SLM are stainless steel, maraging steel, inconel 625 and 718, titanium Ti6Al4V, all being materials with excellent mechanical properties used in most demanding applications. Ti6Al4V being one the most used titanium alloys in aerospace industry for its strength to weight ratio, Inconel as material for jet engines, etc. Most of these materials is difficult to shape using machining and SLM presents great opportunity for it allows production of parts with complex geometry.

Greatest disadvantage of SLM is the fact that it is very time-consuming method and in comparison to conventional machining methods, such as lathe, it is slow. Also, the workplace is limited by its dimensions and of course, it is very expensive to get and to operate.

5.3. Method and materials used for fuel grain

Fuel grains for hybrid rocket engine were made by FFF technology. 3D printer using this method is located at the laboratories of the Department of aerospace engineering of Faculty of mechanical engineering of CTU and it is allowed to students to have study related objects printed on this machine. Used machine is Chinese copy of Ultimaker 2 3D printer, which is suitable for variety of application. With build volume 223x223x205 mm it has more than enough space for printing of the fuel grains. Layer resolution stars from 600 microns up to 20 microns for very detail builds. Build speed for this model is up to 24mm^3/s and travel speed up to 300mm/s. Another reason for choosing FFF is material related. Being one of the cheaper methods using plastics, that can serve as fuel.

PLA (polylactic acid) is thermoplastic made mostly from starch or sugarcane. Having bio origin, it is very commonly stated that PLA is biodegradable. This is true, although process can take very long and highly depends on circumstances, such as access of sunlight, and can even take tens of years. Its easy production, low price, chemical and mechanical properties make it ideal for usage in 3D print. It is most widespread material for 3D printing.

Lactic acid is gained from glucose, acquired through fermentation of starch, and further lactide is derived. Using metal catalysts lactide undergoes polymerization and PLA is formed.

Among disadvantages of PLA is the temperature of glass transition, transition in amorphous materials from solid and hard to a rubber or viscous state, which is at 60-65°C. Objects made of PLA in direct sunlight can therefore become spoiled by the heat. Heat resistant PLA has already been introduced, having the glass transition temperature at around 110°C. Melting temperature is 173-178°C and common printing temperature above 200°C.

Fig. 3 3D printed PLA fuel grains

ABS (acrylonitrile butadiene styrene), amorphous thermoplastic polymer, second favourite material for FFF 3D print. Made by polymerizing acrylonitrile and styrene with presence of polybutadiene ABS combines rigidity and toughness of source materials.

Having mechanical and thermal properties superior to PLA, temperature of glass transition is 105°C and printing temperatures around 250°C, it is viable to use ABS when more durability is required. For example LEGO bricks are made from this material. Of course ABS has some flaws, one of the greatest is thermal expansivity, cooling of the

printed plastic may cause to final product to deform and mostly requires heated printing bed to be used.

Fig. 4 3D printed ABS fuel grain

PET-G (polyethylene terephthalate glycol modified) glycol, added during polymerization, improves PETs mechanical properties to a level similar to ABS, while still having greatest plus of PLA, being easy to print. Print temperatures are same as with ABS.

While other two materials can be burned without any problems, PET-G is considered self extinquishing, therefore it might not work as fuel grain, but will be tested as well.

Fig. 5 3D printed PET-G fuel grain

III. Experimental part

1. Introduction

In this part of thesis will be discussed preparations and experiments that have been conducted. First there are going to be described parts and mechanics of the hybrid rocket engine used for research. Brief characterization of measuring apparatus. After that design process of 3D printable fuel grain used in experiments. In the final part results of various shapes and materials used are discussed.

2. Testing engine

2.1. Parts and description of the engine

Experiments were conducted using a small model-grade hybrid rocket engine. Main body of engine (1) is made of steel tube, with inner diameter of 18.8 mm and outer of 22 mm and length of 152.4 mm. Tube has three notches, two inside at each end of engine for axial securing of the other parts, and on the outside, that has been used for fitting and securing assembled engine in the measuring device.

Other parts include graphene, used because of its thermal properties, made nozzle (2), fuel grain (3). These parts occupy the back section of engine and are separated by aluminium barrier (4). This barrier is shaped to fit in brass piercer (5), which had been later replaced by one made of steel. At the grain side of the barrier a slot for fitting small combustible charge (6) is located, used to burn small plastic disk (7) set under the piercer, to keep fuel and oxidizer section separated. N_2O container (8) is fitted on piercer and held in place at the head end of engine by threaded steel disk (9) with a grub screw (10). Rubber rings (11) are used to seal area around edges of the nozzle, if the fitting is tight enough, as well as space between grain and barrier to prevent undesired leaks of the oxidizer along the walls of the tube. Whole assembly is held together at each end with retaining ring (12) set into the inner notches and one bigger retaining ring (13) set into outer, for additional axial securing in the measuring device.

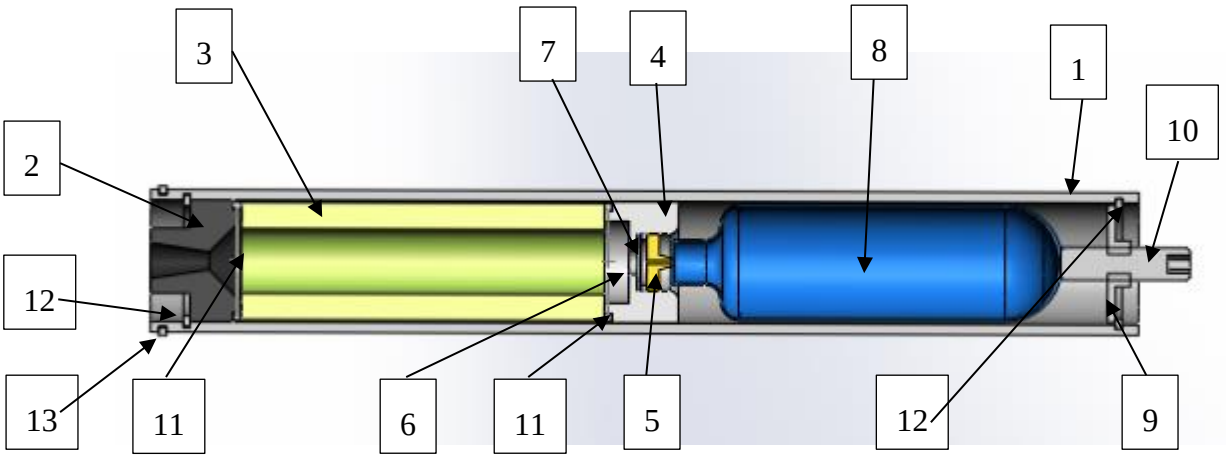

Fig. 6 Model of assembled engine

2.2. Engine mechanics and assembly

To achieve successful blast off first step is to screw grub screw and press N_2O container deeper and to pierce the cap of N_2O container. Oxidizer gas should not been able to flow just yet, but as had been discovered during tests whole assembly was not entirely leak proof and small amount of oxidizer had been able to flow through head end of the rocket engine. Next step is to set ablaze combustible charge, simple piece of firing cord rolled and fitted into slot in the barrier, using electric igniters. Heat generated by charge melts hole in the plastic disk and allows oxidizer to flow into combustion port and thus starting the combustible reaction between fuel grain and oxidizer. Once oxidizer container had been pierced amount of oxidizer flowing into the system can not be optimized or contained. Engine is therefore not throttleable and thrust generated can not be modified during the test.

Method of assembly that had been found as the most efficient goes as follows:

1. Remove all used parts from engine body and clean the inside with cloth to remove all residues of previous combustion.
2. Set fuel grain with sealing ring on the nozzle, grease the nozzle if needed, put the electric igniter in, lead its wires through the nozzle and press into the engine body until nozzle's retaining ring is possible to apply.
3. Put retaining ring in place and make sure that nozzle sits on it, so there is enough space for other parts inside the body.
4. Through head end of the engine push sealing ring on top of the grain.

5. Fit small piece of firing cord, roughly 7 centimetres, into the barrier and place plastic disk with smaller sealing on top of it into the oxidizer side slot.
6. Carefully set the piercer on top of the sealing and slowly lower the barrier on the fuel grain, making sure the piercer does not move out of it is place and is located in the axis of the engine, so proper piercing of the oxidizer container is possible.
7. Put it the container and top it with threaded disk and grub screw.
8. Set in remaining two retaining rings.

3. Measuring apparatus

Initial thought had been to use device already constructed for measuring drag of a small propeller, which had been in laboratories and currently was not in use. After realization that it is way too complex and for purpose of measuring drag of the hybrid rocket engine, simplified system would suffice, eventually new apparatus had been designed and constructed. Welded tube on a thin steel plate screwed with two bolts on aluminium profiles had been used. Tube is cut lengthwise and serves for holding the engine in place, using the outer retaining ring as back stop and two bolts, essentially making it a clamping ring. Strain gauge had been applied on the metal plate to measure its bend after application of force and using software catmanEasy, being calibrated beforehand, thrust generated by the hybrid rocket engine had been measured and ploted during engine run.

Fig. 7 Detail of applied strain gauge

For more information regarding measuring apparatus, its preparation design and construction, seek out bachelor thesis Measurement of thrust of small hybrid rocket engine (Měření tahu malého hybridního raketového motoru) written by my colleague Jakub Podzimek of CTU, with whom we had closely cooperated on our theses and whose thesis focuses in detail on the measurements technique and various useful information about it may be found there.

4. Design and production of fuel grain

All fuel grains initial models had been designed as parametric models using CAD software SolidWorks, under student license acquired from CTU Faculty of Mechanical engineering. Native .sldprt files had been saved as .stl files, files utilizable by most of the 3D printers, and supplied to Ing. Tomáš Čenský Ph.D., tutor in charge of laboratories 3D printer, who had printed them.

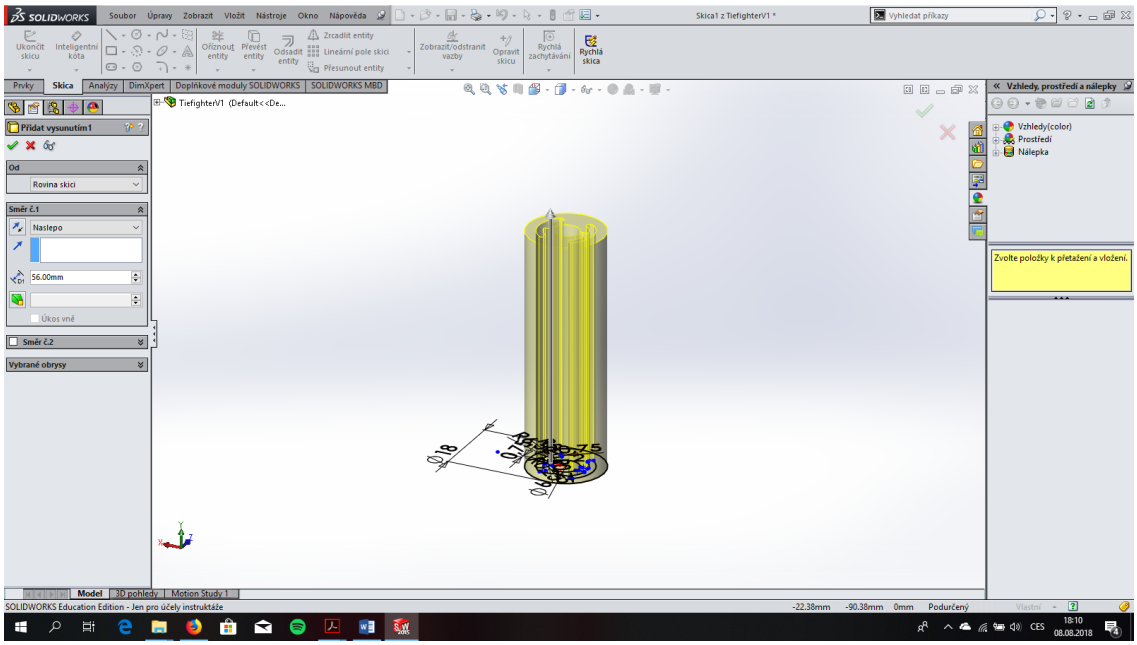

Fig. 8 Design in process in SolidWorks CAD software

By measuring fuel grains provided with the engine, exact dimensions were known and based on these first shape had been designed as a copy of provided fuel grains, therefore as a tube with inner diameter of 10mm, outer 18mm and approximate length of 56mm. For other designs I had found inspiration either in shapes and designs used in common practice of hybrid rocketry, literature and for some I had used my imagination, because 3D printing is suitable method for production of such small objects with complex geometries or internal structure. Taking in account fact, that PLA, ABS and PET-G, being the most common materials for 3D print, and all being available for use in Aeronautics department of Mechanical engineering faculty, these had been chosen as materials for fuel grains.

After first specimen had been printed out (PLA tube) and after consulting with Ing. Čenský printing technology had been slightly adjusted. First piece of fuel grain had been printed at full length of 56 mm. This had been proved to be inefficient, print took long time and this way low number of grains could had been produced at same time. Taking in account advice from Ing. Čenský CAD models had been adjusted to grains with ½ length for further prints. Two halves of the fuel grain had always been loaded in the engine, secured with duct tape if needed to ensure matching of the geometry, for more complex combustion port shapes. This way more grains could had been produced at the same time and greatly decreasing production time needed for printing of the grain. 3D

printer is also needed for other projects under the Aeronautics department and therefore could not had been occupied all the time with making of fuel grains.

3D print had not always been perfect and some of the printed pieces required small adjustments to ensure smooth insert in the engine during assembly. Some fuel grains had to be grinded or trimmed of excess material interfering with other parts during assembling procedure. Mostly this had occurred with ABS fuel grains, where its thermal expansion caused minor flaws with the shape.

5. Experiment description

In the following paragraph process of experiment will be depicted. First thing that had been done is the successful assembly of hybrid rocket engine, more thoroughly described in previous part of the thesis. Before putting the fuel grain and oxidizer container into the engine, both is weighted. Same after the experiment, amount of burned mass is vital for computations of specific impulse generated by engine. Measuring device, attached to stand made of protruded aluminium profiles, carried outside the Aeronautics laboratories to testing area. Laptop with catmanEasy software [10] and spyder system had been brought to testing area next and connected to measuring device. Battery powered ignition system with switch to start launch. In earlier stages of experiments set of four AA batteries had been used, after they ran dry, car battery had been attached as powering cell of the system. Rocket engine had been mounted in the clamping ring and bolts tightened to ensure firm hold of the engine body. After checking the setting of the engine electric igniter wires are connected to launch control system. CatmanEasy software had been launched next with the program calibrated and prepared for this measurements.

Fig. 9 Measuring station prepared for experiment

With everything ready for conducting of the experiment, grub screw is tightened. Light hissing of the leaking oxidizer is the sing of pierced container and measurement can be started on the laptop. After software starts to measure data switch is pressed and igniter ignited, starting of the engine. After engine run is ended, usually under two seconds, measurement is terminated and data saved.

Fig. 10 Engine during run, on the left mounted in measuring apparatus, on the right in the old measuring stand

Before dismounting the engine from clamping ring it is needed to wait some time and let the engine body cool. Dismounted engine is disassembled at the working bench inside laboratories and cleaned, if required. Engine is now ready for next assembly and another experiment with different fuel grain.

Over fifty experiments had been conducted overall using different fuel grain shapes and materials.

5.1. Difficulties experienced

Not all experiments that had been done were successful. In the early stages, during unmeasured tests, oxidizer leaks had occurred in approximately 1/3 of attempts. Caused probably by improper pierce of the oxidizer container, oxidizer leaked through unsealed head end of the engine right after tightening of the grub screw. In the attempts to come this problem began to be less occurring and probably was caused by insufficient tightening of the screw or by poor assembly of the engine. As we had become more proficient in the engine assembly and firing this had occurred more and more rarely.

Other trouble during tests had been the electric igniters. On few occasions the head of the igniter had lost contact with fuse at some point either during assembly or during process of mounting the engine into the clamping ring of measuring device. When switch had been pressed and igniter went off, it was too far from fuse to cause its ignition, thus the plastic disc had been kept unharmed and oxidizer prevented from flowing into the combustion port. Whole engine had to be dismounted and disassembled. Change of oxidizer tank was possible without removing all the parts but igniter head was too big to fit through nozzle so it had to be removed and whole engine assembled from the beginning as it is described in the previous paragraphs.

The most severe failure posing a real threat had been overpressure in oxidizer section without any way of leak allowed to oxidizer. Probably improper pierce of container caused oxidizer to flow into the oxidizer section of the engine, but in this case leaking was not allowed. Rising pressure forced head end retaining ring to leave its place and launched the oxidizer container out at dangerously high speed hitting and discarded case of one of the laboratory machine. Engine body with other parts still placed within had been launched in opposite direction and landed on the construction site neighbouring at the time with Aeronautics department laboratories. On the second occasion this had happened clamping ring had been tighten in more thorough manner and engine body stayed firmly set in the measuring apparatus and oxidizer container hit wall of the laboratories. No real damage had been caused by either of these failures and similar problem had not occurred since.

Fig. 11 Aftermath of the overpressure

During test of one PLA fuel grain malfunction in oxidizer flow caused overall mass flux to be below "cooking" limit, described in theoretical part of the thesis. As effect of this very poor thrust had been generated and partly melted fuel hurled through nozzle. Heat had not been sufficient to pyrolyze the fuel grain surface properly and decent combustion had not started. After cooling of the grain the nozzle had been choked up with the remains of the grain and had to be carefully cleared.

Manipulation with the nozzle had been proved to be tricky, especially during disassembly of the engine. Graphene is a brittle material and the heat generated in combustion sometimes had melted rubber sealing ring and burned on its remains on both the nozzle and engine body, making it hard to put apart. One of the supplied nozzles had been destroyed in the process of disassembly, while few others suffered minor damage with no real effect on the overall engine properties.

6. Measurements results

In this chapter drag of the hybrid rocket engine with use of different fuel grain shapes and materials will be discussed. During the measuring process metal plate with strain gauge had highly oscillated and in order to provide more easily readable data results had been, with kind help of Ing. Kučera, smoothed using DIAdem software for managing and post processing data. In charts listed below always original data along with smoothed are displayed.

Results are sorted based on the shape of fuel grain, in the first section results of tube shaped grain from all materials are listed for comparison. In following sections fuel

grain with combustion port in shape of cross, circle with connected chambers, five pointed star and tree are presented. Included and compared are performances of all 3D printed grains. Last chapter is covering various prototype shapes, which had been printed only from PLA.

Charts are followed with computations of regression rate and specific impulse. Assuming the regression rate as linear function and using Eq(4) regression rate can be figure up with following expression:

$$r = \frac{R_1 - R_2}{t}$$

Eq. (6) Simplified regression rate

R_1 = precombustion radius [mm]

R_2 = diameter after radius [mm]

t = time of the engine run [s]

r = regression rate [mm/s]

Specific impulse had been computed using following expression:

$$I_{sp} = \frac{A_{chart}}{m_b}$$

Eq. (7) Specific impulse

I_{sp} = specific impulse [N.s/kg]

A_{chart} = area under charted curvature [N.s]

m_b = mass burned during combustion (oxidizer and grain) [kg]

$$m_b = m_{b,ox} + m_{b,gr}$$

Eq. (8) Burned mass

$m_{b,ox}$ = mass of burned oxidizer [kg]

$m_{b,gr}$ = mass of burned oxidizer [kg]

Area under charted curvature had been detected using software and is taking in account only part of the curve during the engine run. As an engine run is meant a time

period in which thrust is generated. We can see in the charts that start of the thrust is clearly visible. With the end of the run it is more complicated. Thrusts end is decide either by visible drop in the chart and in measured data or when the data start to oscillate around a certain point. In the charts we can also see that after the run, values of the thrust are slightly higher than in the pre-run state. This is caused by deformation of the steel plate during the test and this values are not taken in account in the following computations of the specific impulse.

Computations done using expressions Eq. (5) and Eq. (6) and are not explicitly mentioned. All results are stated in tables.

Regression rate is not stated at every fuel shape. For some fuel grains exact measurement of the key dimension after combustion was simply not possible, mostly because of the state in which fuel grain was after the experiment. In the Eq. (4) is stated that regression is computed using pre and post combustion radius, other than grains with circular combustion ports sometime offer no measureable radius, therefore different dimension may be used.

6.1. Tube

Being the simplest shape it is only fitting to begin with it. Drag over time charts of various materials, included those shipped with hybrid engine, are listed below and compared with those of 3D printed tubes. Dimension measured for regression rate computation is tubes diameter in this case. Regression rate therefore states, change of diameter in millimetres per second.

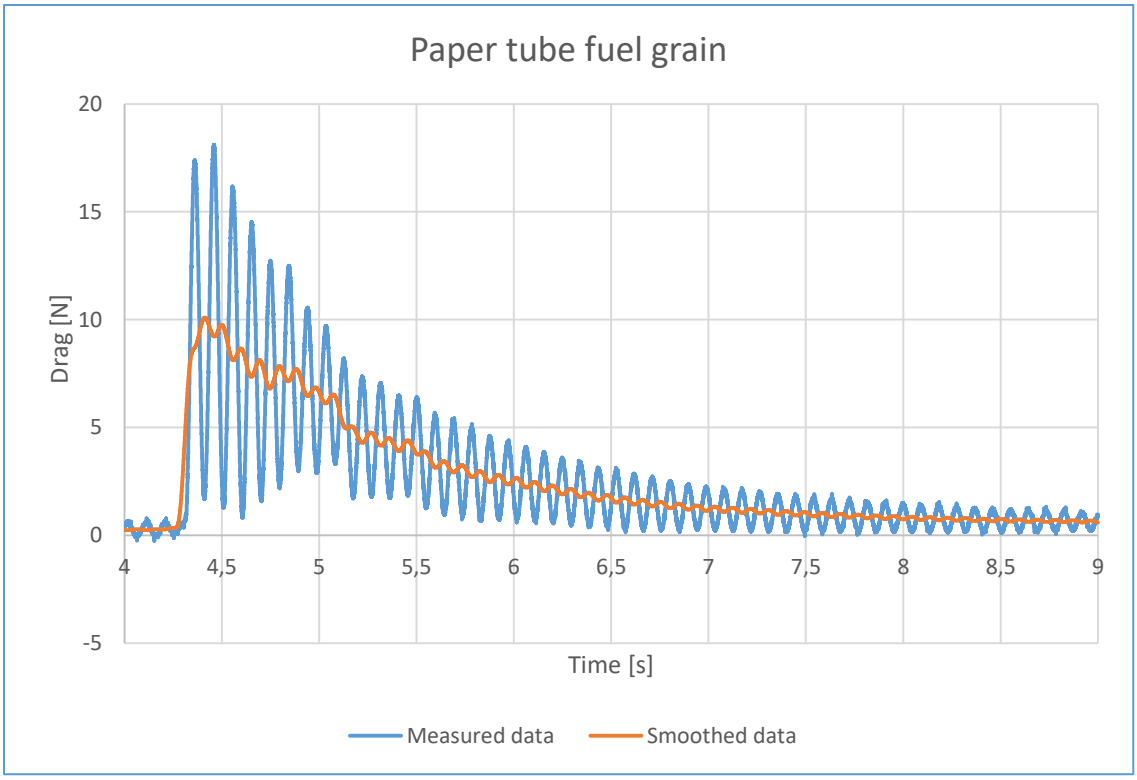

Chart 1: Thrust generated by paper tube fuel grain over time.

Maximal Thrust [N]	Duration of the thrust [s]	Area under curve [N.s]	Specific impulse [N.S/kg]	Regression rate [mm/s]
10,1	2	10,23	973,85	2,21

Table 2: Thrust and specific impulse related values for paper tube fuel grain.

Combusted grain weight [g]	Combusted oxidizer weight [g]	Pre-combustion dimension [mm]	After-combustion dimension [mm]
3	7,5	9	13,5

Table 3: Grain and oxidizer related values for paper tube fuel grain.

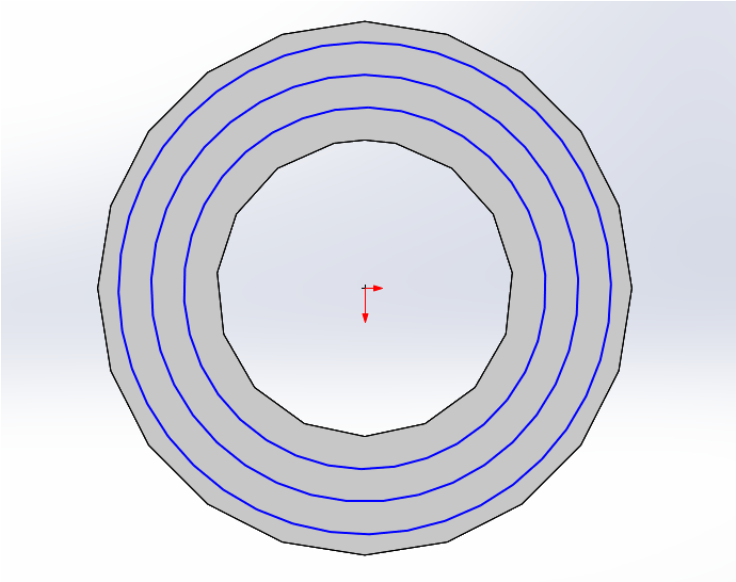

Fig. 12 Paper tube regression rate visualized

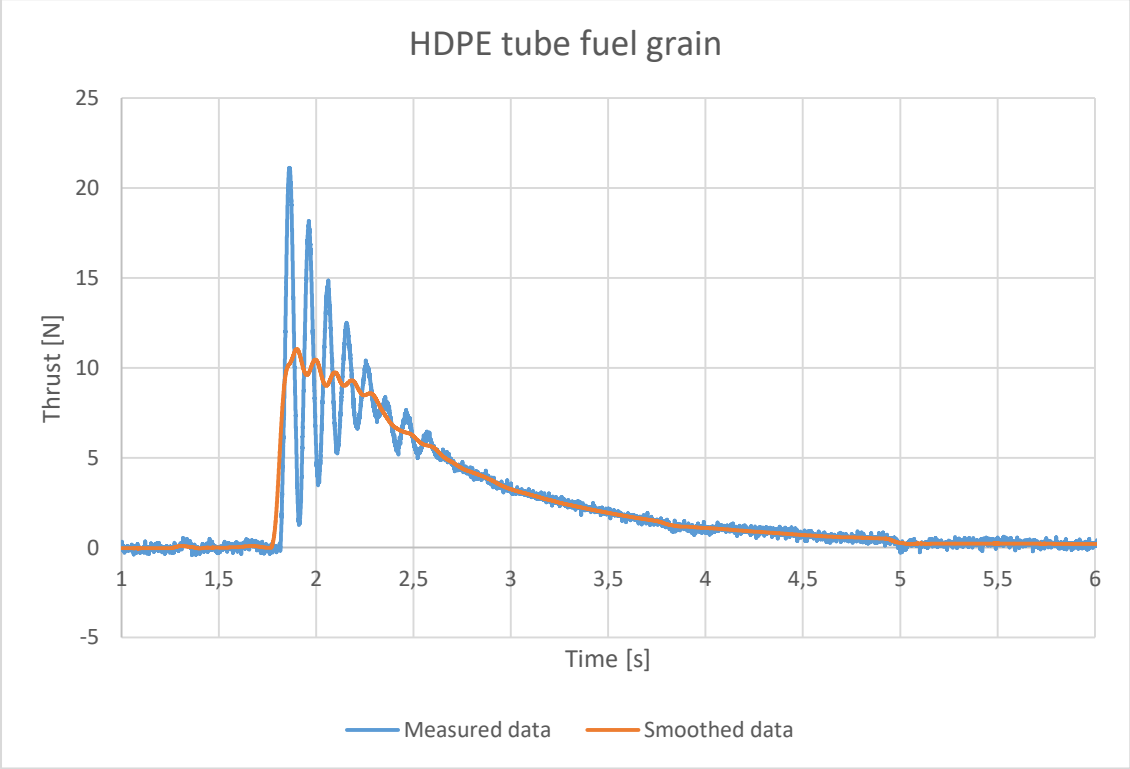

Chart 2: Thrust generated by HDPE tube fuel grain over time.

Maximal Thrust [N]	Duration of the thrust [s]	Area under curve [N.s]	Specific impulse [N.S/kg]	Regression rate [mm/s]
11	2,12	10,24	1124,99	0,59

Table 4: Thrust and specific impulse related values for HDPE tube fuel grain.

Combusted grain weight [g]	Combusted oxidizer weight [g]	Pre-combustion dimension [mm]	After-combustion dimension [mm]
1,4	7,6	9	10,26

Table 5: Grain and oxidizer related values for HDPE tube fuel grain.

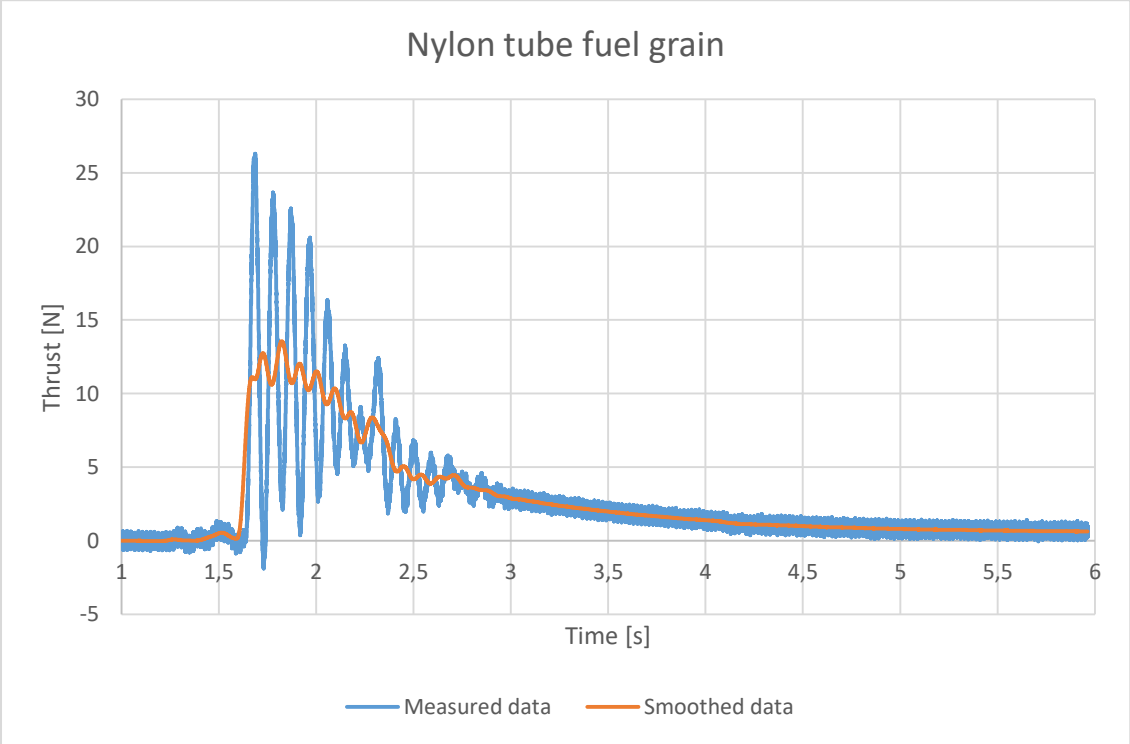

Chart 3: Thrust generated by Nylon tube fuel grain over time

Maximal Thrust [N]	Duration of the thrust [s]	Area under curve [N.s]	Specific impulse [N.S/kg]	Regression rate [mm/s]
13,5	2,4	12	1165,12	0,64

Table 6: Thrust and specific impulse related values for Nylon tube fuel grain.

Combusted grain weight [g]	Combusted oxidizer weight [g]	Pre-combustion dimension [mm]	After-combustion dimension [mm]
2,7	7,6	9,1	10,64

Table 7: Grain and oxidizer related values for Nylon tube fuel grain.

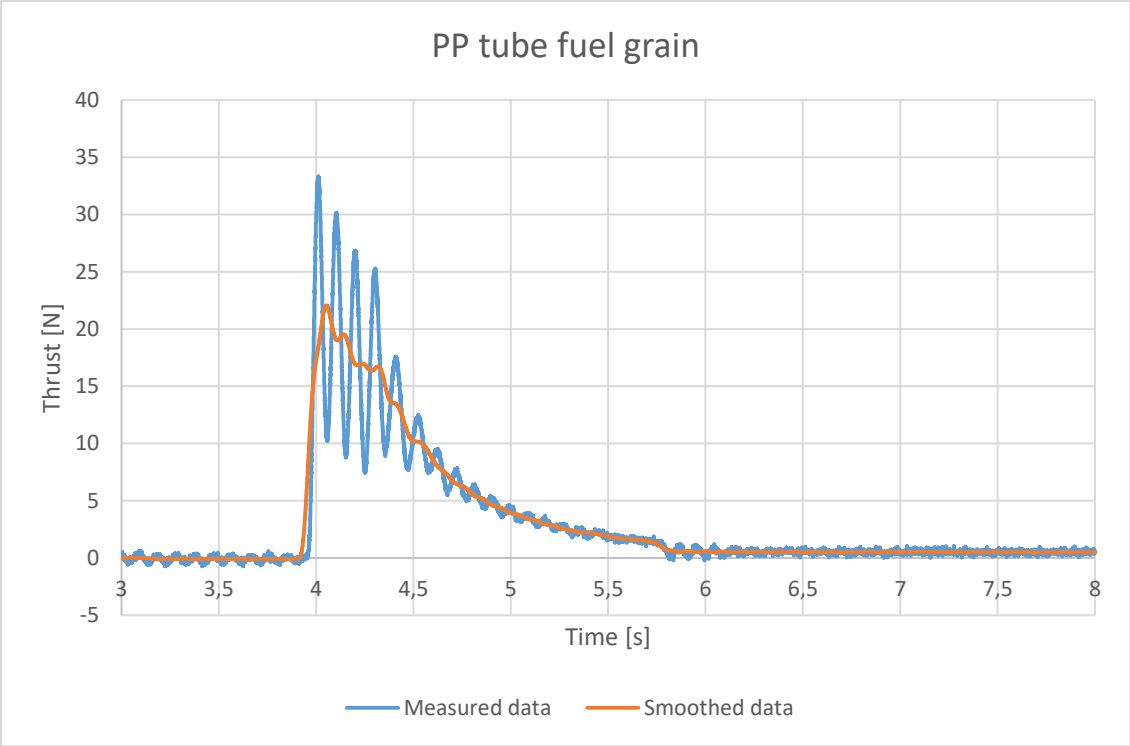

Chart 4: Thrust generated by PP tube fuel grain over time

Maximal Thrust [N]	Duration of the thrust [s]	Area under curve [N.s]	Specific impulse [N.S/kg]	Regression rate [mm/s]
22	1,9	14,11	1700,63	0,92

Table 8: Thrust and specific impulse related values for PP tube fuel grain.

Combusted grain weight [g]	Combusted oxidizer weight [g]	Pre-combustion dimension [mm]	After-combustion dimension [mm]
1,3	7	9	10,75

Table 9: Grain and oxidizer related values for PP tube fuel grain.

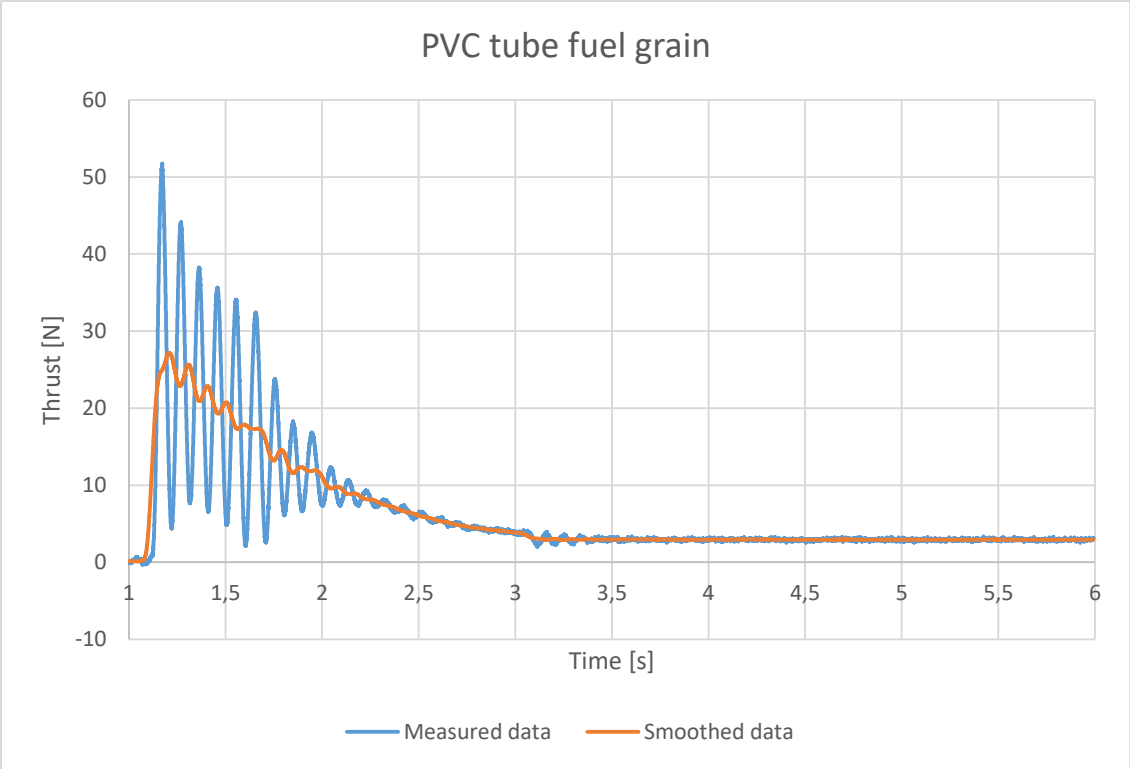

Chart 5: Thrust generated by PVC tube fuel grain over time

Maximal Thrust [N]	Duration of the thrust [s]	Area under curve [N.s]	Specific impulse [N.S/kg]	Regression rate [mm/s]
27	2	23,04	2075,92	1,29

Table 10: Thrust and specific impulse related values for PVC tube fuel grain.

Combusted grain weight [g]	Combusted oxidizer weight [g]	Pre-combustion dimension [mm]	After-combustion dimension [mm]
3,5	7,6	9	11,6

Table 11: Grain and oxidizer related values for PVC tube fuel grain.

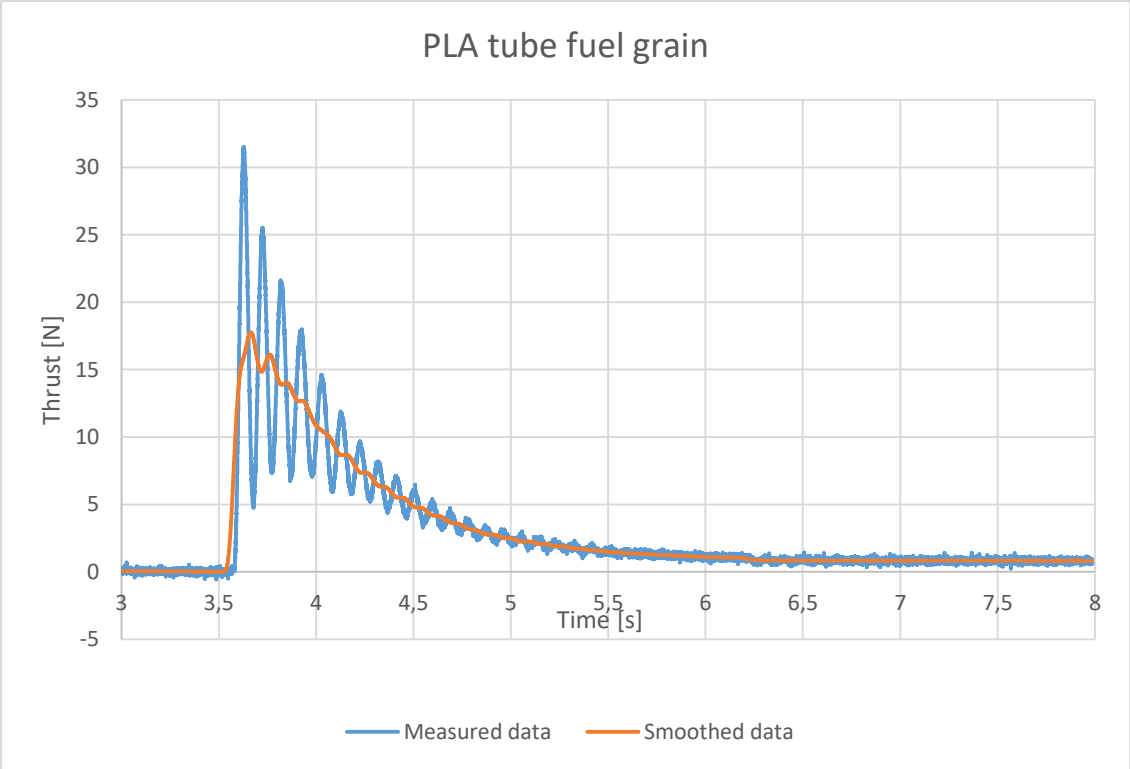

Chart 6: Thrust generated by PLA tube fuel grain over time

Maximal Thrust [N]	Duration of the thrust [s]	Area under curve [N.s]	Specific impulse [N.S/kg]	Regression rate [mm/s]
17,75	2,4	13,18	1365,65	0,65

Table 12: Thrust and specific impulse related values for PLA tube fuel grain.

Combusted grain weight [g]	Combusted oxidizer weight [g]	Pre-combustion dimension [mm]	After-combustion dimension [mm]
2,35	7,3	10	11,56

Table 13: Grain and oxidizer related values for PLA tube fuel grain.

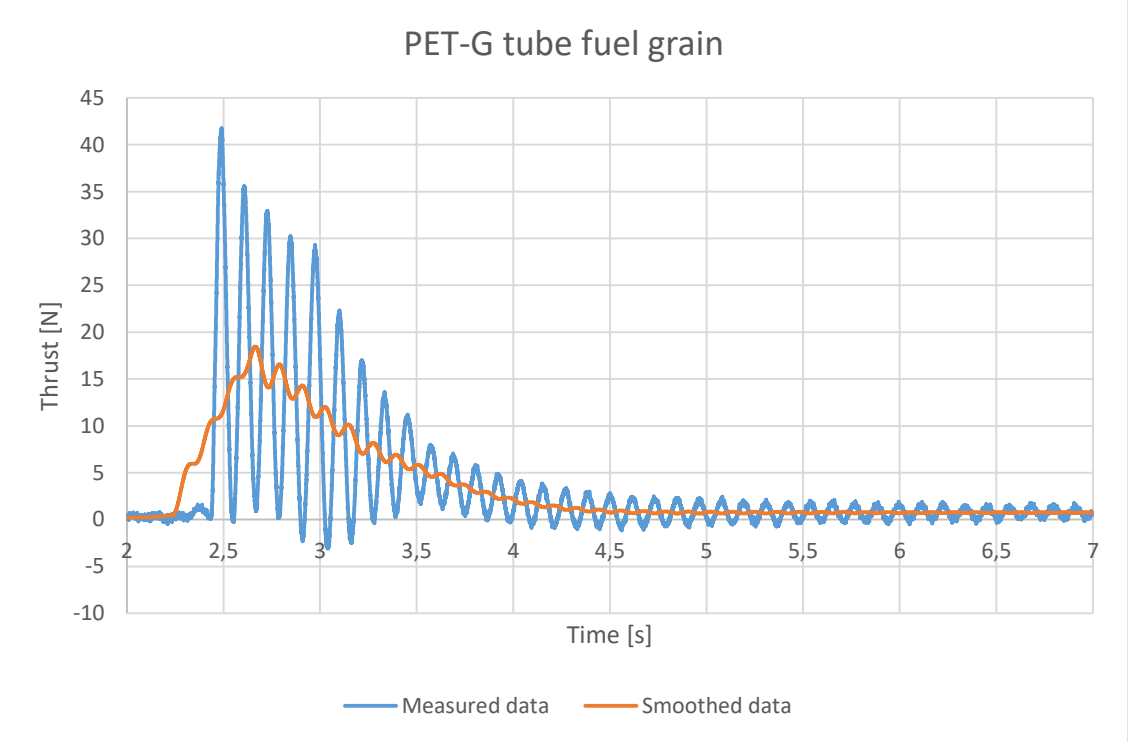

Chart 7: Thrust generated by PET-G tube fuel grain over time

Maximal Thrust [N]	Duration of the thrust [s]	Area under curve [N.s]	Specific impulse [N.S/kg]	Regression rate [mm/s]
18,5	2	15,35	1564,35	0,47

Table 14: Thrust and specific impulse related values for PET-G tube fuel grain.

Combusted grain weight [g]	Combusted oxidizer weight [g]	Pre-combustion dimension [mm]	After-combustion dimension [mm]
2,4	7,4	10	10,94

Table 15: Grain and oxidizer related values for PET-G tube fuel grain.

	Paper	HDPE	PVC	PP	PLA	PET-G	Nylon
I_{sp}	973,85	1124,99	2075,92	1700,63	1365,65	1564,35	1165,12
Max. Thrust	10,1	11	27	22	17,75	18,5	13,5

Table 16: Comparison of I_{sp} and maximal provided thrust for different grain materials

6.2. Cross

Cross shaped combustion port with small circular hole in the middle, in order to pull through igniter without any trouble, should according to theory provide higher initial thrust slowly regressing to zero.

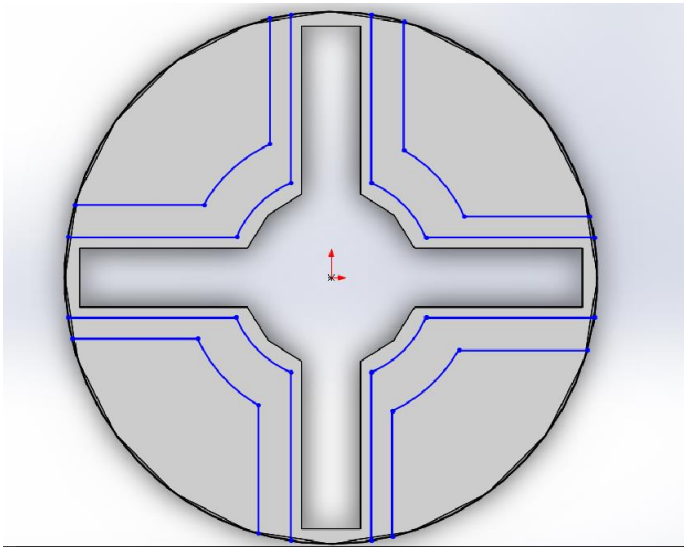

Fig. 13 Cross fuel grain regression visualized

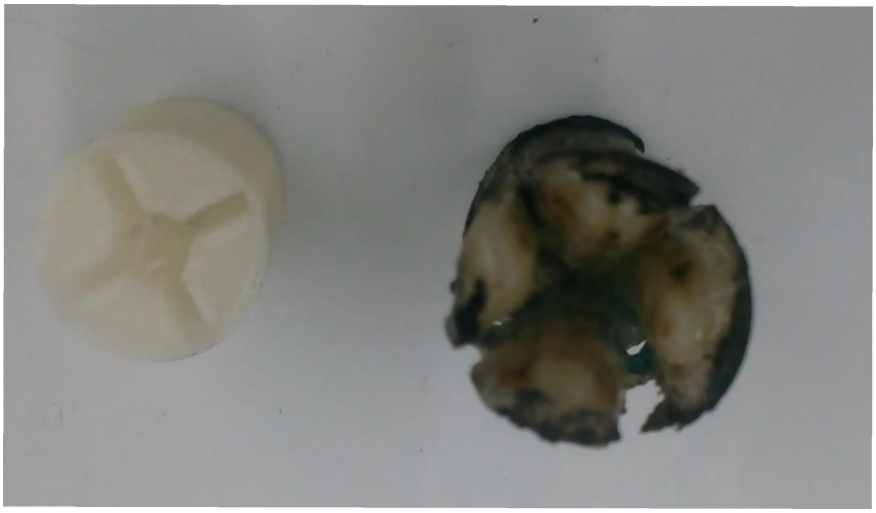

Fig. 14 Cross fuel grain, pre-combustion left, post right, PLA

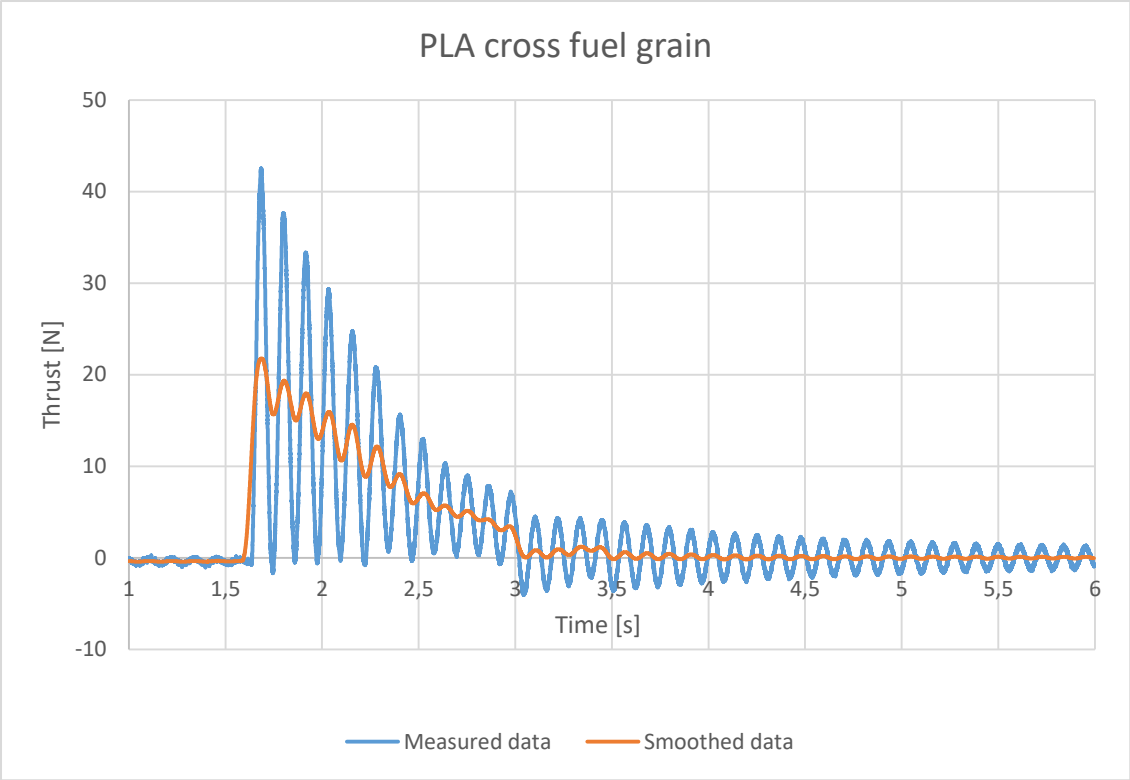

Chart 8: Thrust generated by PLA cross shaped fuel grain over time

Maximal Thrust [N]	Duration of the thrust [s]	Area under curve [N.s]	Specific impulse [N.S/kg]	Regression rate [mm/s]
21,75	1,47	14,16	1401,58	x

Table 15: Thrust and specific impulse related values for PLA cross shaped fuel grain.

Combusted grain weight [g]	Combusted oxidizer weight [g]	Pre-combustion dimension [mm]	After-combustion dimension [mm]
2,7	7,4	x	x

Table 16: Grain and oxidizer related values for PLA cross shaped fuel grain.

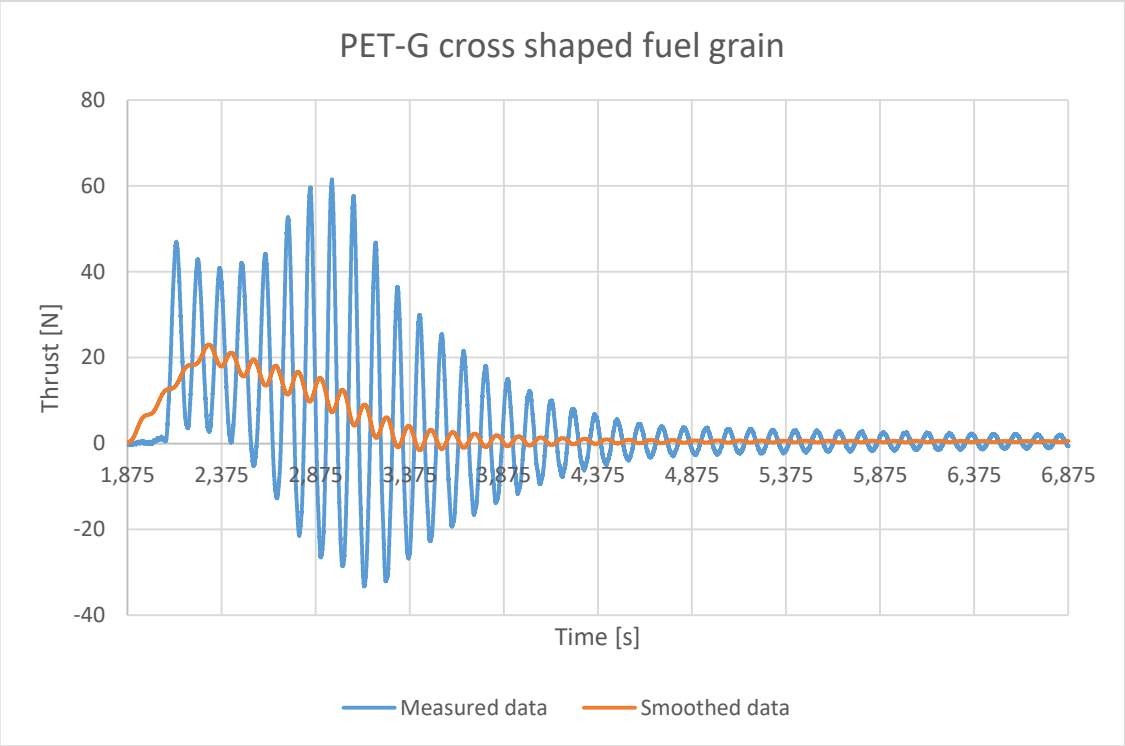

Chart 9: Thrust generated by PET-G cross shaped fuel grain over time

Maximal Thrust [N]	Duration of the thrust [s]	Area under curve [N.s]	Specific impulse [N.S/kg]	Regression rate [mm/s]
16,5	1,58	13,41	1289,8	X

Table 17: Thrust and specific impulse related values for PET-G cross shaped fuel grain.

Combusted grain weight [g]	Combusted oxidizer weight [g]	Pre-combustion dimension [mm]	After-combustion dimension [mm]
2,9	7,5	X	X

Table 18: Grain and oxidizer related values for PET-G cross shaped fuel grain.

6.3. Star

Fuel grain shape reminding of five pointed star should offer thrust not as high as other shapes might offer but sustainable for certain amount of time.

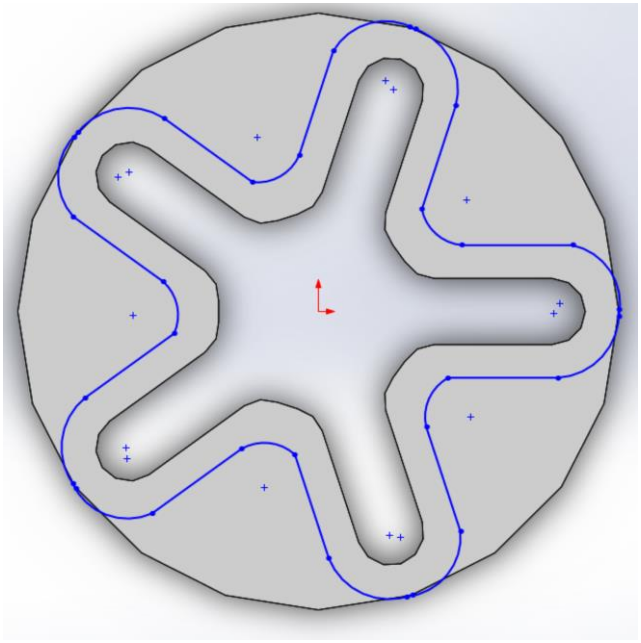

Fig. 15 Star shaped combustion port regression rate visualization

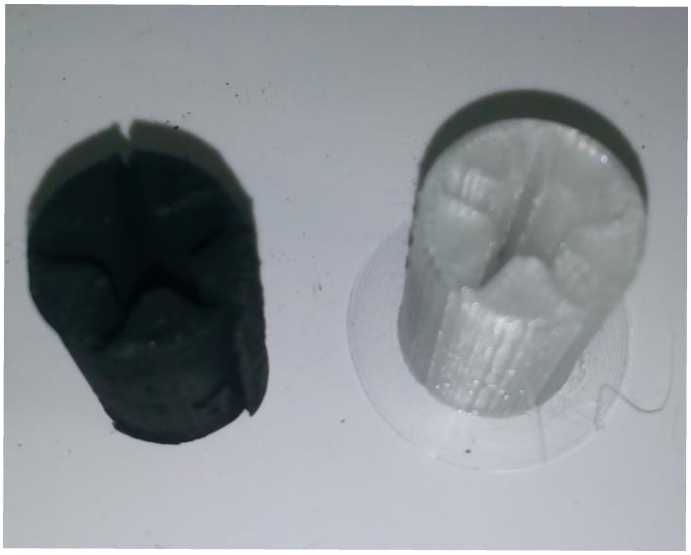

Fig. 16 Star shaped combustion port, after combustion left, pre right, PET-G

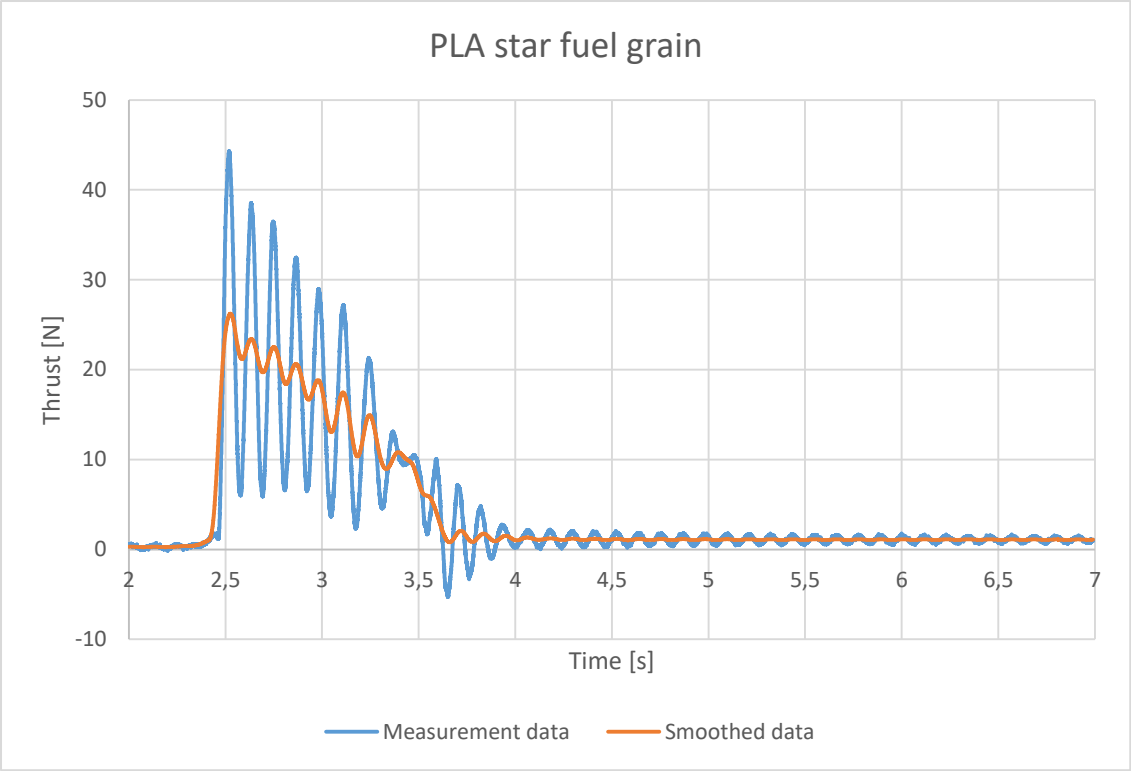

Chart 10: Thrust generated by PLA star shaped fuel grain over time

Maximal Thrust [N]	Duration of the thrust [s]	Area under curve [N.s]	Specific impulse [N.S/kg]	Regression rate [mm/s]
26	1,26	18,15	1852,21	1,08

Table 19: Thrust and specific impulse related values for PLA star shaped fuel grain.

Combusted grain weight [g]	Combusted oxidizer weight [g]	Pre-combustion dimension [mm]	After-combustion dimension [mm]
2,3	7,5	2	0,64

Table 20: Grain and oxidizer related values for PLA star shaped fuel grain.

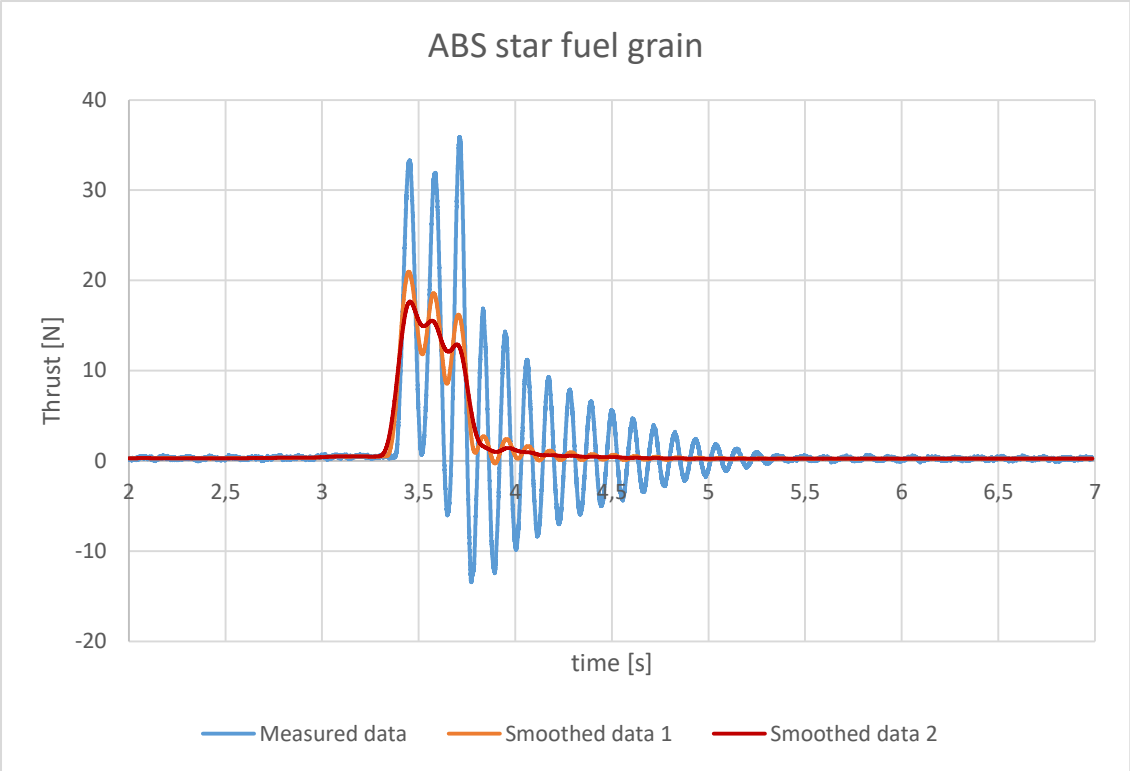

Chart 11: Thrust generated by ABS star shaped fuel grain over time

Maximal Thrust [N]	Duration of the thrust [s]	Area under curve [N.s]	Specific impulse [N.S/kg]	Regression rate [mm/s]
21	0,56	5,75	701,24	1,58

Table 21: Thrust and specific impulse related values for ABS star shaped fuel grain.

Combusted grain weight [g]	Combusted oxidizer weight [g]	Pre-combustion dimension [mm]	After-combustion dimension [mm]
0,8	7,4	2	1,124

Table 22: Grain and oxidizer related values for ABS star shaped fuel grain.

6.4. Circular combustion chamber with two side ports

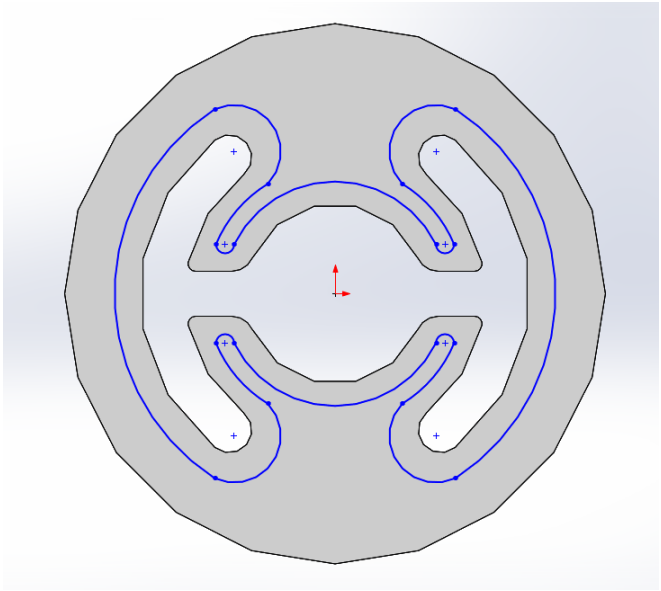

Fig. 17 Regression rate visualization

Fig. 18 left pre-combustion fuel grain, right post, PLA

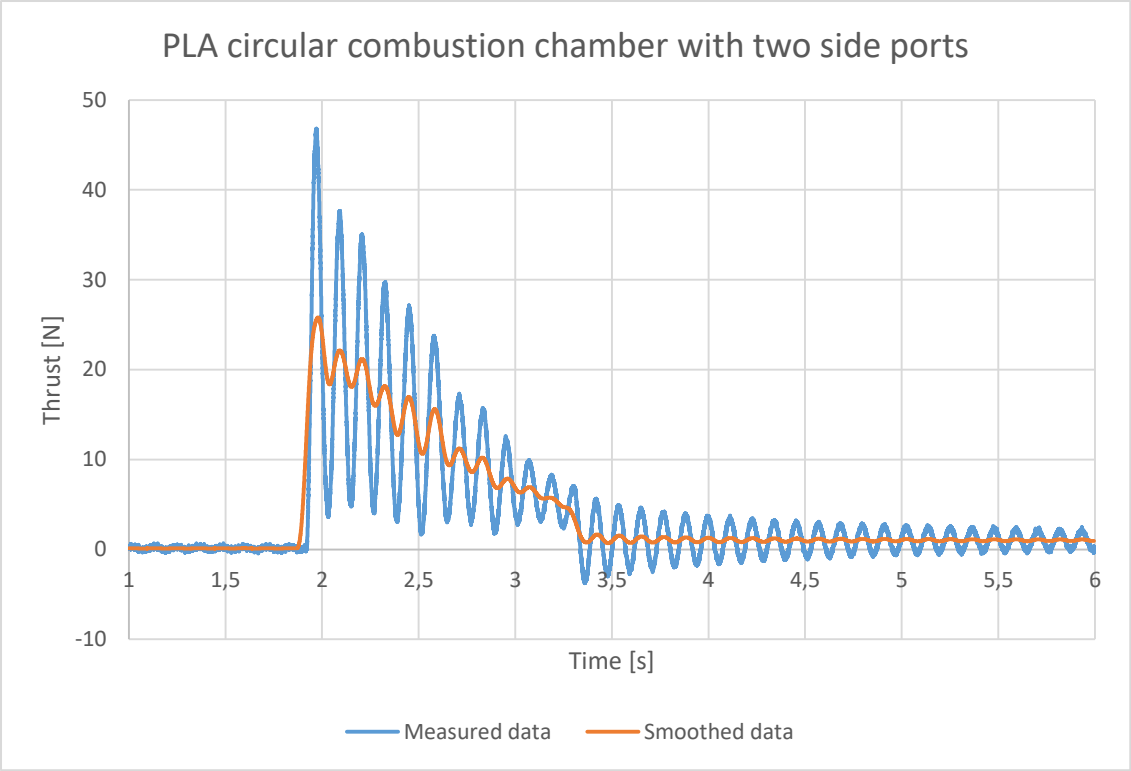

Chart 12: Thrust generated by PLA circular combustion port with two side ports fuel grain over time

Maximal Thrust [N]	Duration of the thrust [s]	Area under curve [N.s]	Specific impulse [N.S/kg]	Regression rate [mm/s]
26	1,52	17,86	1733,93	0,67

Table 23: Thrust and specific impulse related values for PLA circular combustion port with two side ports fuel grain.

Combusted grain weight [g]	Combusted oxidizer weight [g]	Pre-combustion dimension [mm]	After-combustion dimension [mm]
2,9	7,4	13	14,02

Table 24: Grain and oxidizer related values for PLA circular combustion port with two side ports fuel grain.

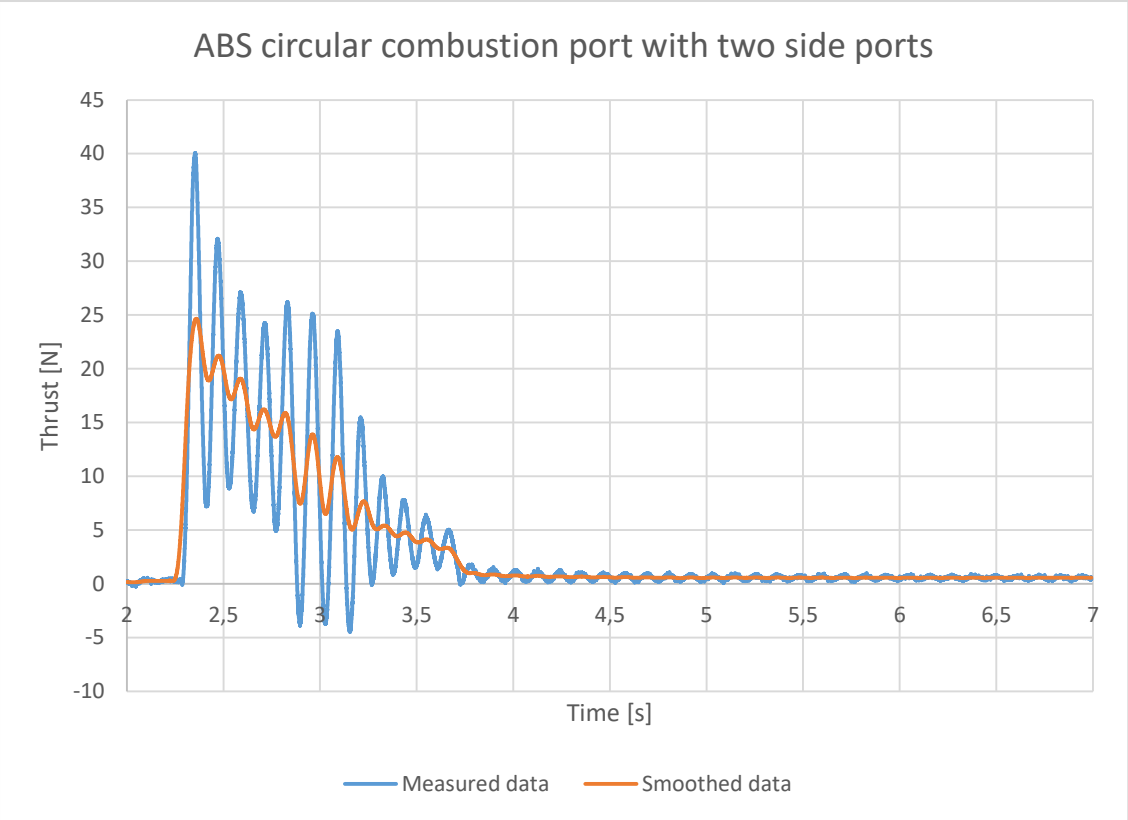

Chart 13: Thrust generated by ABS circular combustion port with two side ports fuel grain over time

Maximal Thrust [N]	Duration of the thrust [s]	Area under curve [N.s]	Specific impulse [N.S/kg]	Regression rate [mm/s]
24,5	1,52	15,69	1584,83	0,53

Table 25: Thrust and specific impulse related values for ABS circular combustion port with two side ports fuel grain.

Combusted grain weight [g]	Combusted oxidizer weight [g]	Pre-combustion dimension [mm]	After-combustion dimension [mm]
2,5	7,4	13	13,8

Table 26: Grain and oxidizer related values for circular ABS combustion port with two side ports fuel grain.

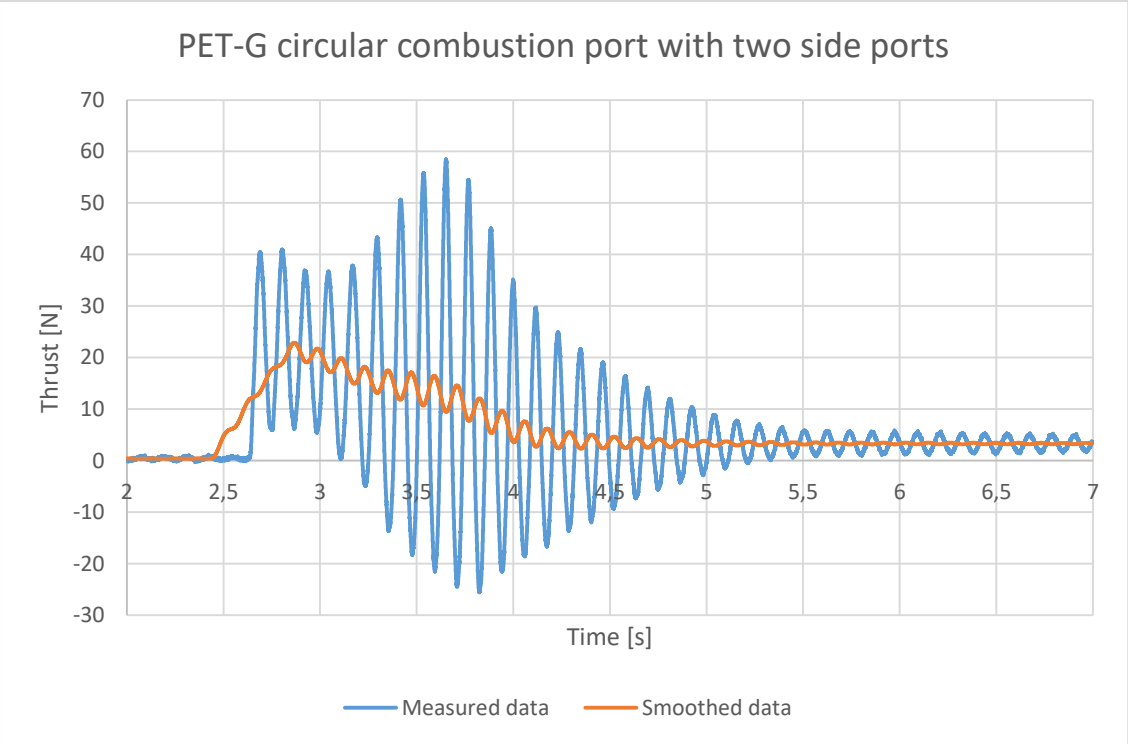

Chart 14: Thrust generated by PET-G circular combustion port with two side ports fuel grain. over time

Maximal Thrust [N]	Duration of the thrust [s]	Area under curve [N.s]	Specific impulse [N.S/kg]	Regression rate [mm/s]
22,5	1,67	18,45	1464,78	0,2

Table 27: Thrust and specific impulse related values for PET-G circular combustion port with two side ports fuel grain.

Combusted grain weight [g]	Combusted oxidizer weight [g]	Pre-combustion dimension [mm]	After-combustion dimension [mm]
5,1	7,5	2,5	2,16

Table 28: Grain and oxidizer related values for PET-G circular combustion port with two side ports fuel grain.

6.5. Root shaped cross-section

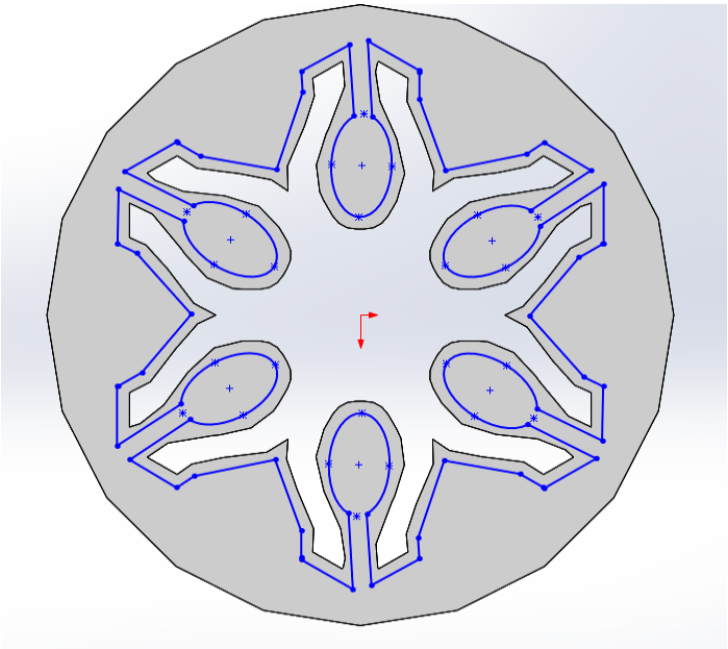

Fig. 19 Regression rate visualization

Fig. 20 left post-combustion fuel grain, right pre, PLA

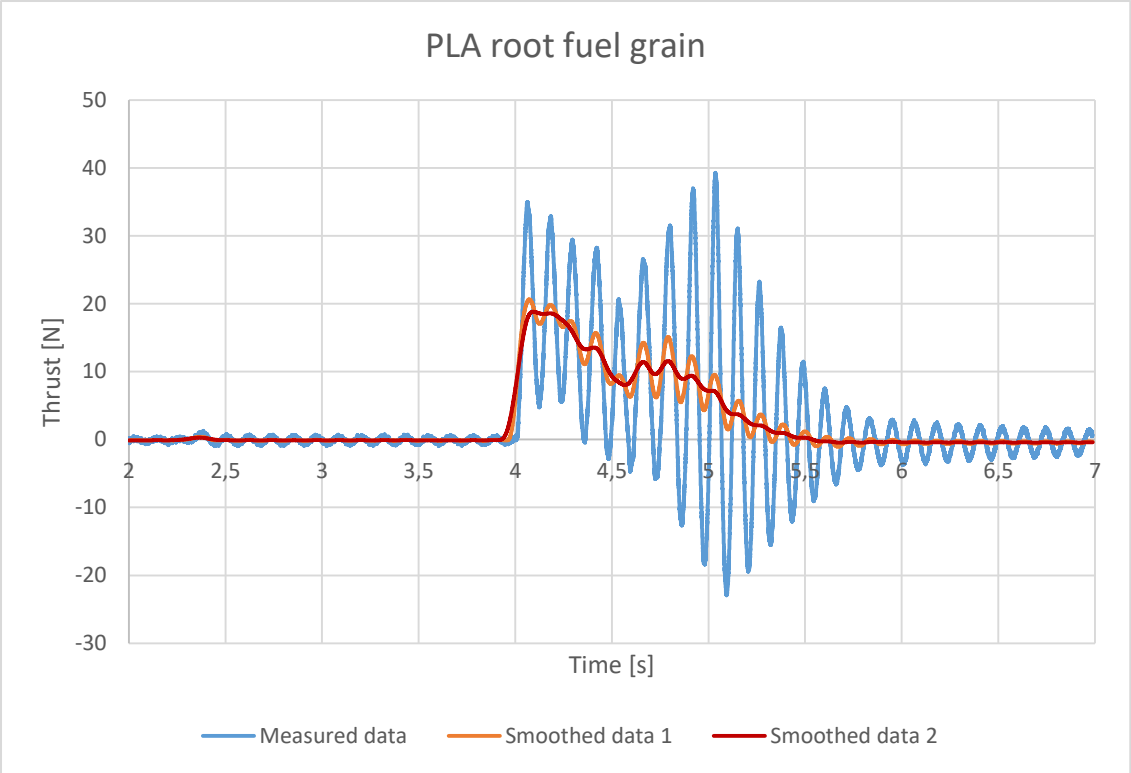

Chart 15: Thrust generated by PLA root shaped fuel grain over time

Maximal Thrust [N]	Duration of the thrust [s]	Area under curve [N.s]	Specific impulse [N.S/kg]	Regression rate [mm/s]
19	1,47	13,94	1003,37	X

Table 29: Thrust and specific impulse related values for PLA root shaped fuel grain.

Combusted grain weight [g]	Combusted oxidizer weight [g]	Pre-combustion dimension [mm]	After-combustion dimension [mm]
6,5	7,4	X	X

Table 30: Grain and oxidizer related values for PLA root shaped fuel grain.

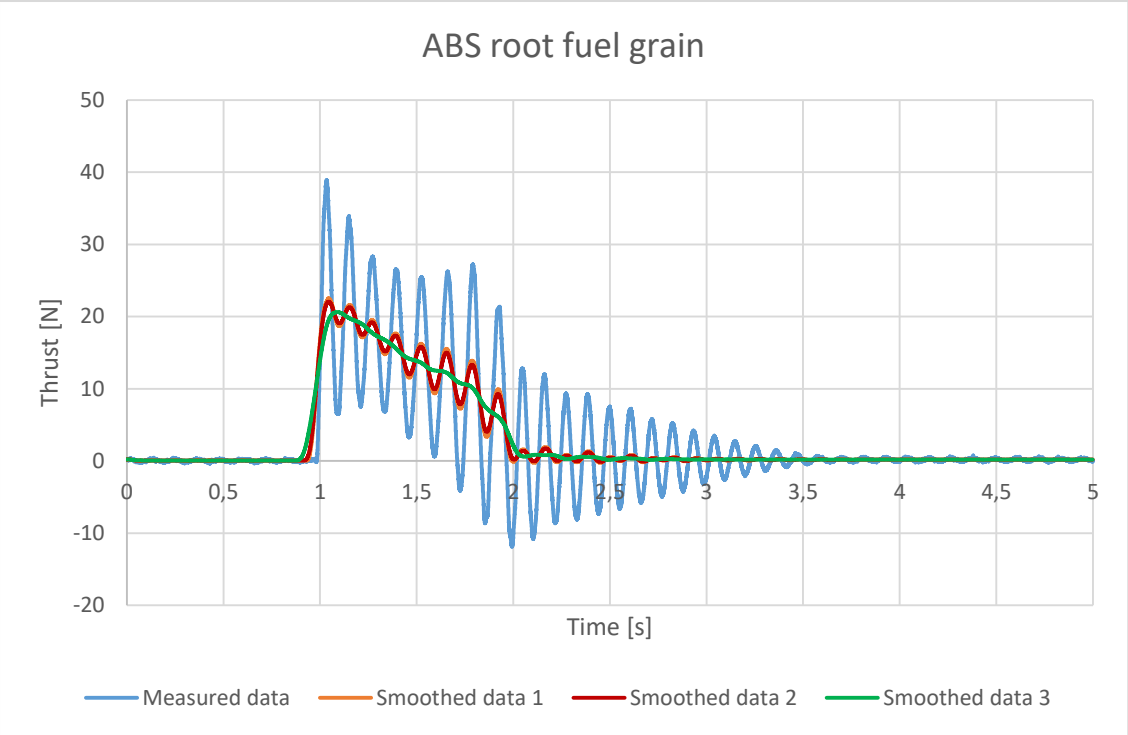

Chart 16: Thrust generated by ABS root shaped fuel grain over time

Maximal Thrust [N]	Duration of the thrust [s]	Area under curve [N.s]	Specific impulse [N.S/kg]	Regression rate [mm/s]
20,5	1,9	14,3	1248,59	X

Table 31: Thrust and specific impulse related values for ABS root shaped fuel grain.

Combusted grain weight [g]	Combusted oxidizer weight [g]	Pre-combustion dimension [mm]	After-combustion dimension [mm]
4,1	7,4	X	X

Table 32: Grain and oxidizer related values for ABS root shaped fuel grain.

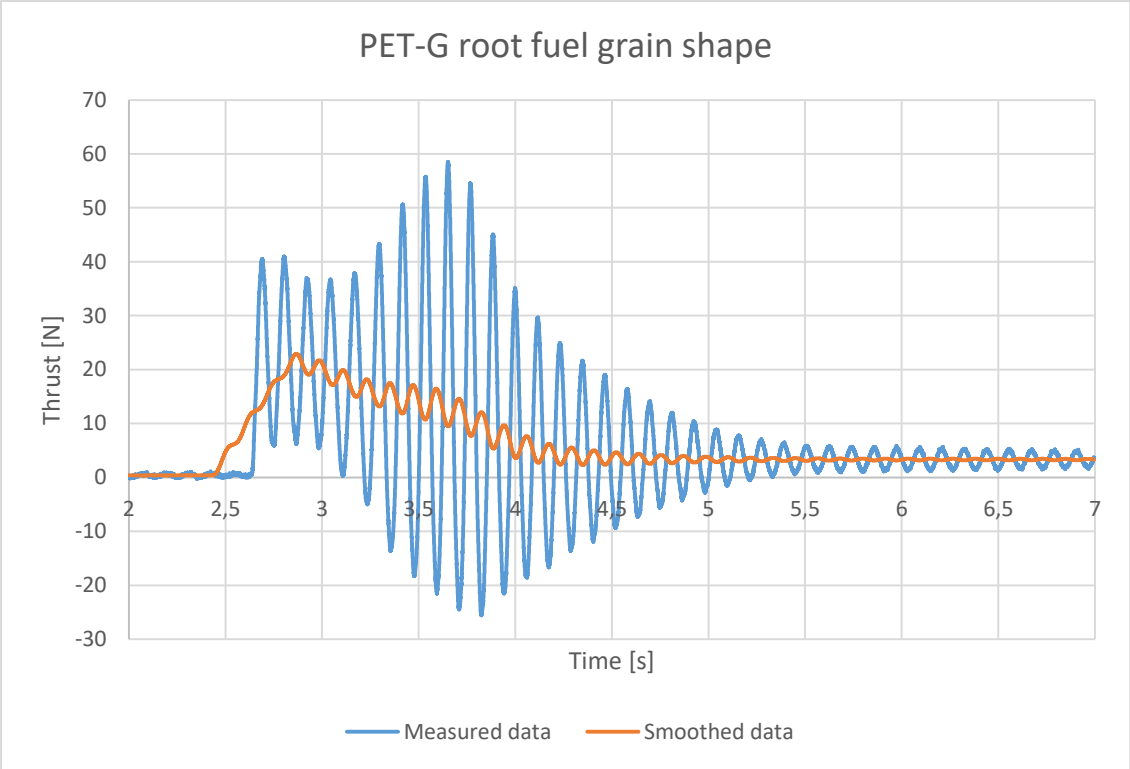

Chart 17: Thrust generated by PET-G root shaped fuel grain over time

Maximal Thrust [N]	Duration of the thrust [s]	Area under curve [N.s]	Specific impulse [N.S/kg]	Regression rate [mm/s]
22,9	1,52	23,02	2112,48	X

Table 33: Thrust and specific impulse related values for PET-G root shaped fuel grain.

Combusted grain weight [g]	Combusted oxidizer weight [g]	Pre-combustion dimension [mm]	After-combustion dimension [mm]
3,5	7,4	X	X

Table 34: Grain and oxidizer related values for PET-G root shaped fuel grain.

6.6. Various fuel grain prototypes from PLA

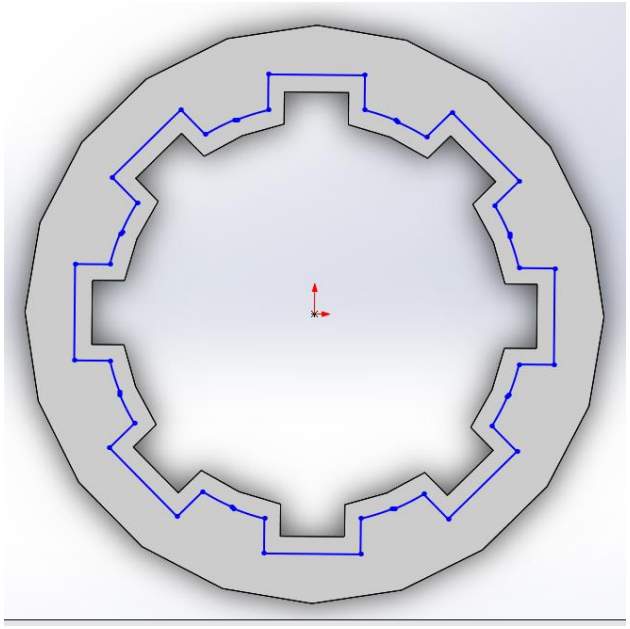

Fig. 21 Cogwheel fuel grain, with visualized 1st step of regression

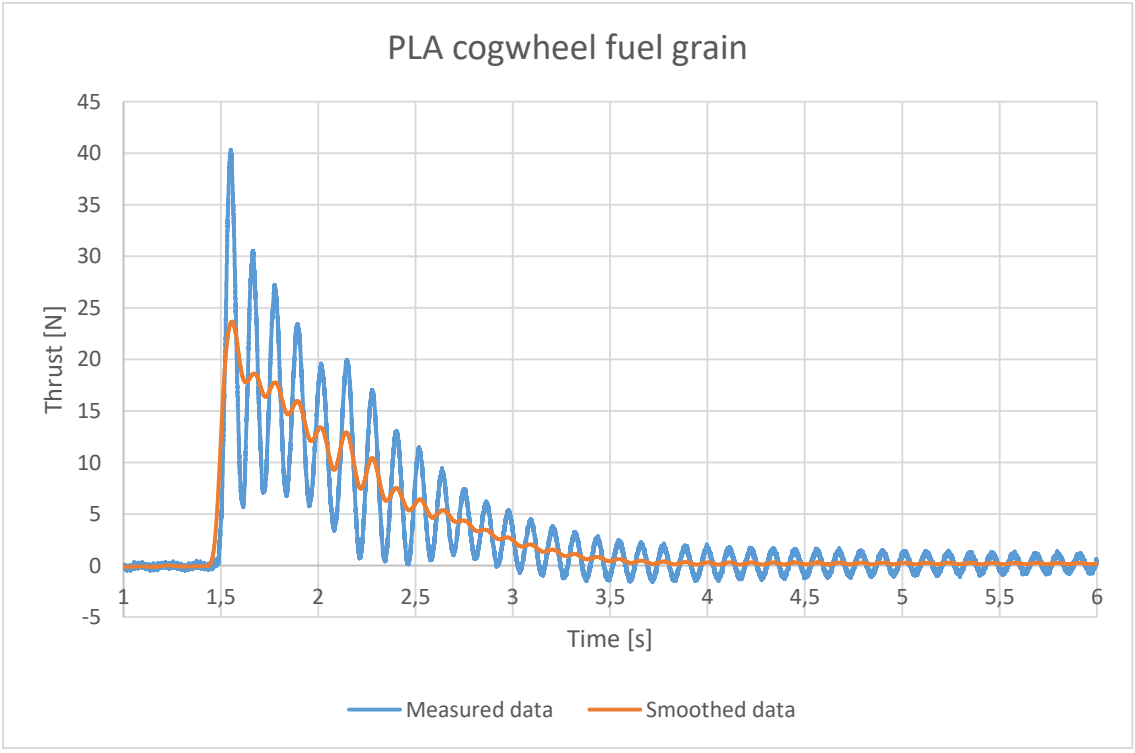

Chart 18: Thrust generated by PLA cogwheel shaped fuel grain over time

Maximal Thrust [N]	Duration of the thrust [s]	Area under curve [N.s]	Specific impulse [N.S/kg]	Regression rate [mm/s]
23,5	2,05	15,96	1662,86	0,83

Table 35: Thrust and specific impulse related values for PLA cogwheel shapedfuel grain.

Combusted grain weight [g]	Combusted oxidizer weight [g]	Pre-combustion dimension [mm]	After-combustion dimension [mm]
2,2	7,4	1,75	0,04

Table 36: Grain and oxidizer related values for PLA cogwheel shaped fuel grain.

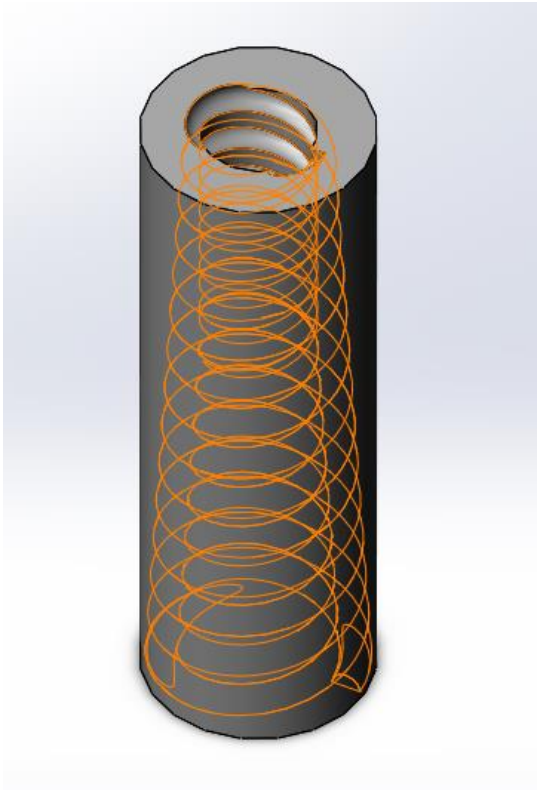

Fig. 22 Circular combustion port with highlighted internal double helix

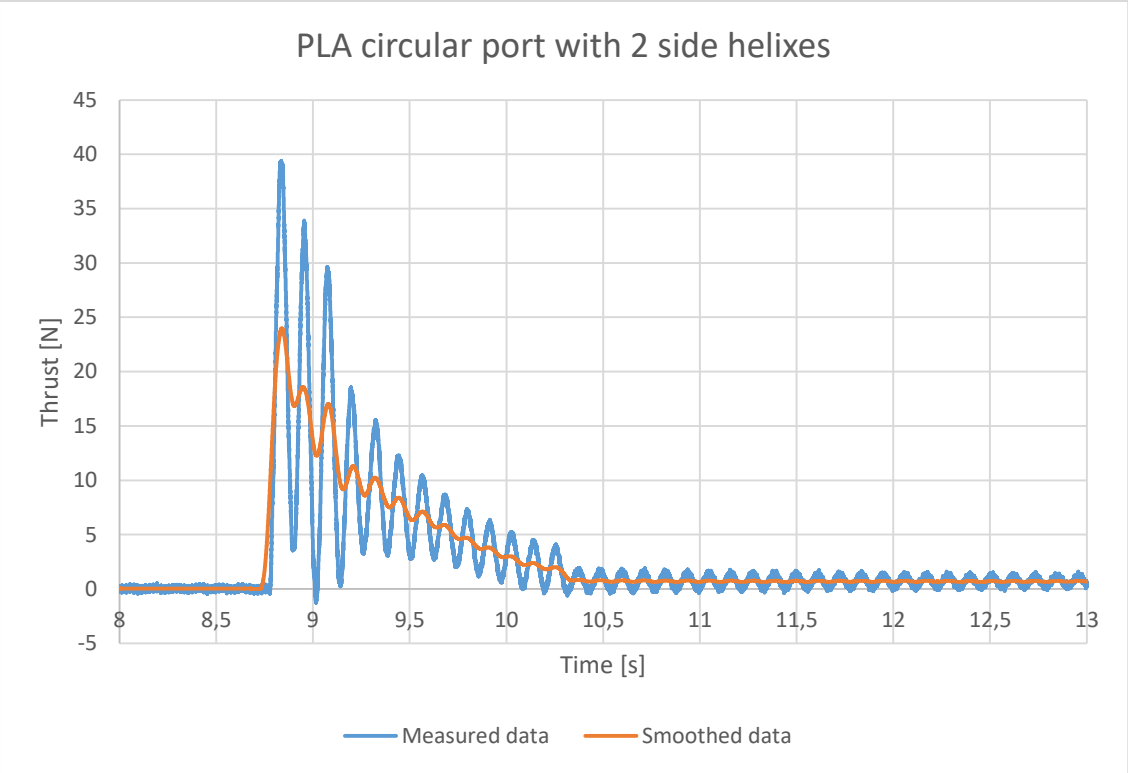

Chart 19: Thrust generated by PLA circular combustion port shaped fuel grain with two helical side ports over time

Maximal Thrust [N]	Duration of the thrust [s]	Area under curve [N.s]	Specific impulse [N.S/kg]	Regression rate [mm/s]
24	1,64	12,71	1199,27	0,55

Table 37: Thrust and specific impulse related values for PLA circular combustion port shaped fuel grain with two helical side ports fuel grain.

Combusted grain weight [g]	Combusted oxidizer weight [g]	Pre-combustion dimension [mm]	After-combustion dimension [mm]
3,2	7,4	10	10,9

Table 38: Grain and oxidizer related values PLA circular combustion port shaped fuel grain with two helical side ports fuel grain.

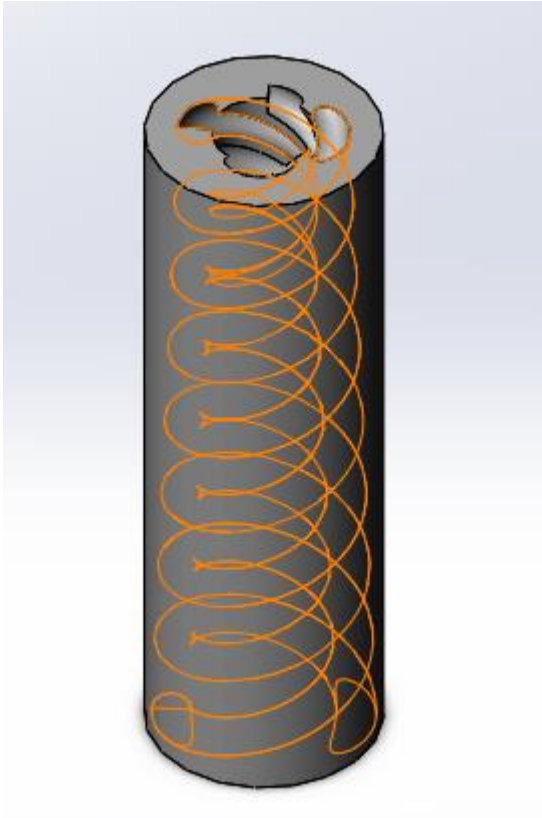

Fig. 23 Circular combustion port with highlighted internal double helix, second double helix is not visible

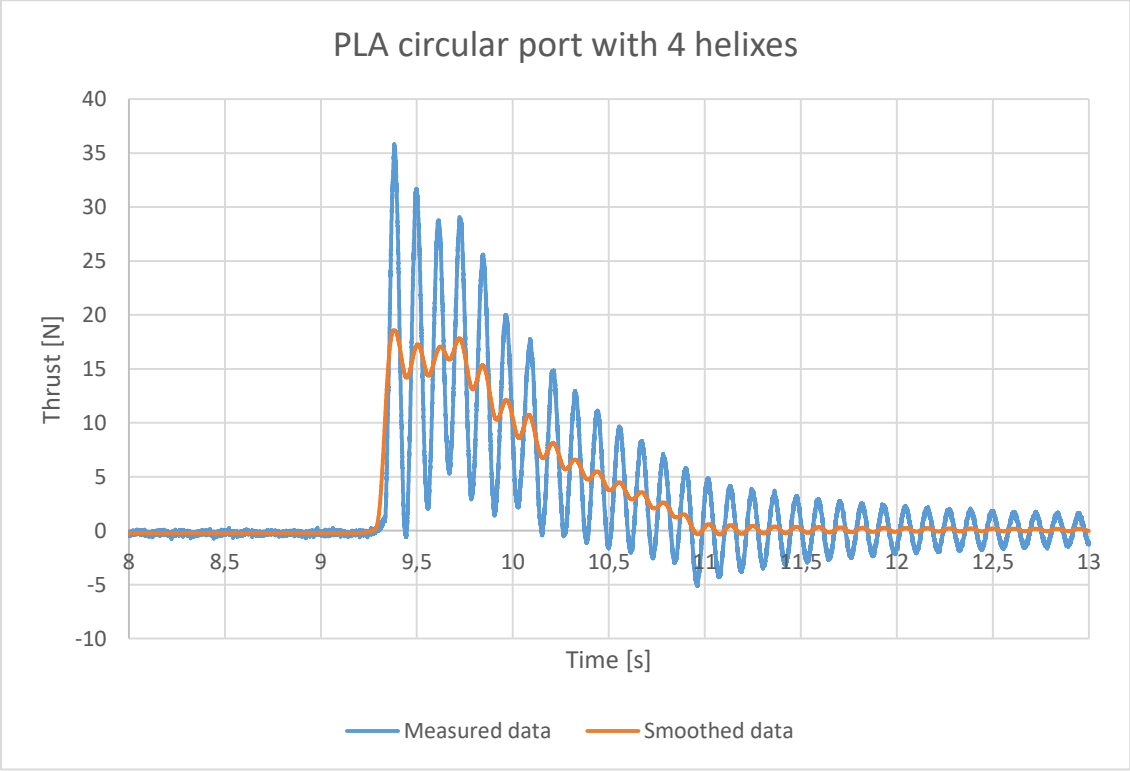

Chart 20: Thrust generated by PLA circular combustion port shaped fuel grain with four helical side ports over time

Maximal Thrust [N]	Duration of the thrust [s]	Area under curve [N.s]	Specific impulse [N.S/kg]	Regression rate [mm/s]
18,5	1,76	14,8	1332,57	1,41

Table 39: Thrust and specific impulse related values for PLA circular combustion port shaped fuel grain with four helical side ports fuel grain.

Combusted grain weight [g]	Combusted oxidizer weight [g]	Pre-combustion dimension [mm]	After-combustion dimension [mm]
3,7	7,4	10	12,48

Table 40: Grain and oxidizer related values for PLA circular combustion port shaped fuel grain with four helical side ports fuel grain.

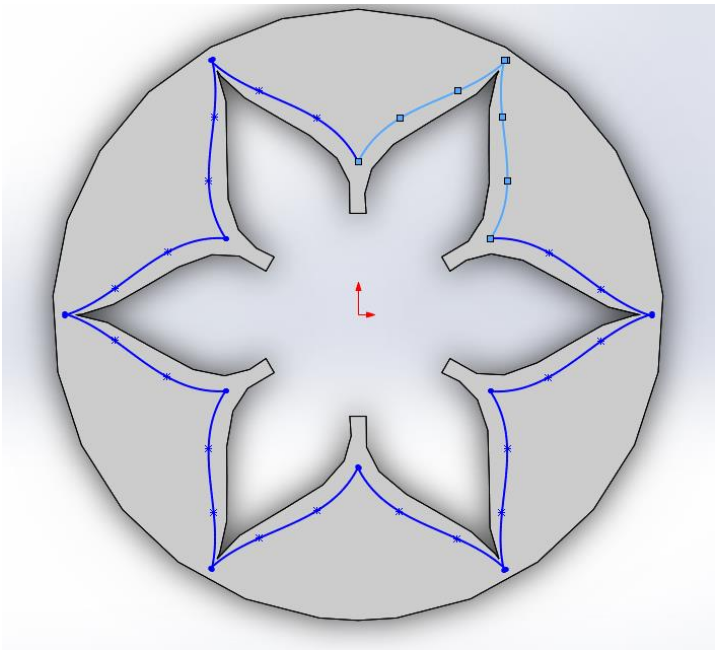

Fig. 24 Flower, combustion port shaped like 6 flower petals, with visualized 1st step of regression

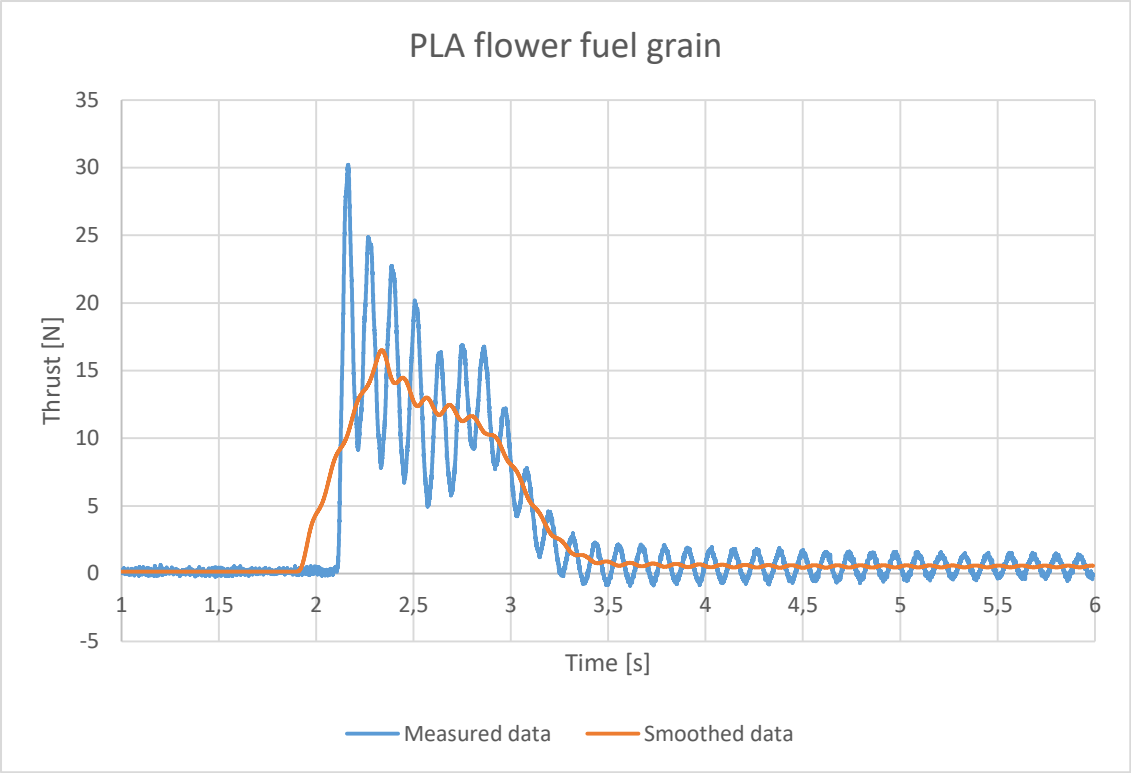

Chart 21: Thrust generated by PLA flower shaped fuel grain over time

Maximal Thrust [N]	Duration of the thrust [s]	Area under curve [N.s]	Specific impulse [N.S/kg]	Regression rate [mm/s]
16,5	1,58	13,41	1289,8	X

Table 41: Thrust and specific impulse related values for PLA flower shaped fuel grain.

Combusted grain weight [g]	Combusted oxidizer weight [g]	Pre-combustion dimension [mm]	After-combustion dimension [mm]
2,9	7,5	X	X

Table 42: Grain and oxidizer related values for PLA flower shaped fuel grain.

Fig. 25 Improved version of root fuel grain shape, root_2

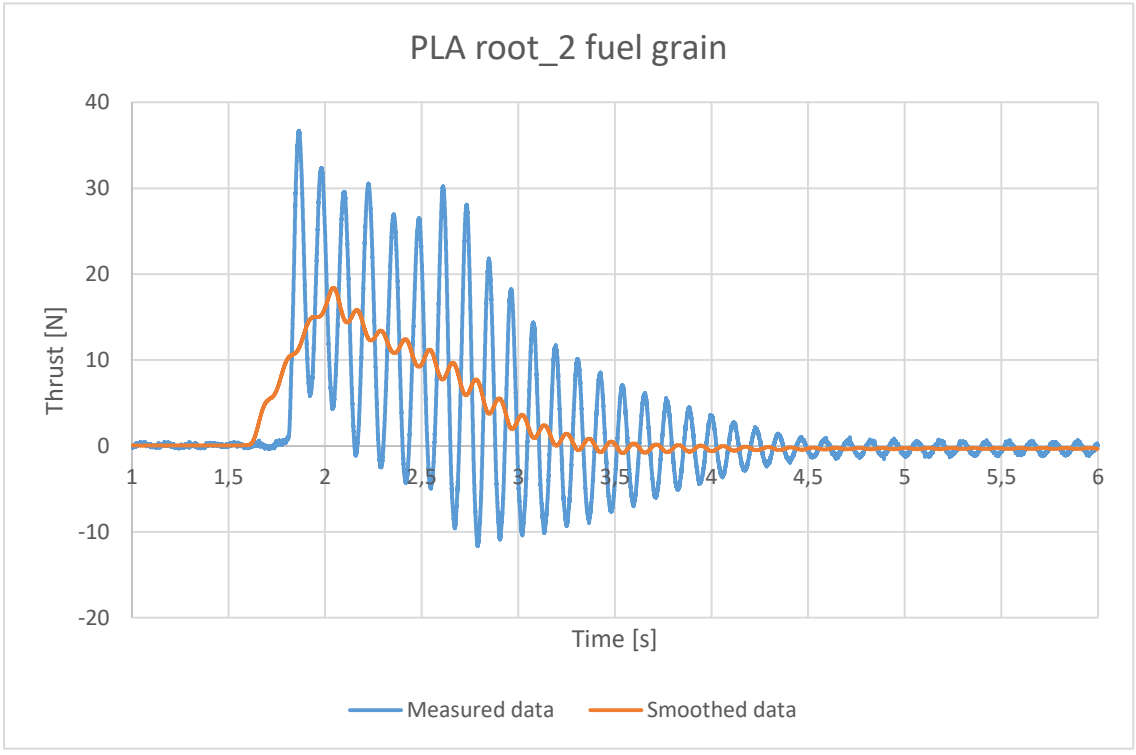

Chart 22: Thrust generated by PLA root_2, modified version of tree, shaped fuel grain over time

Maximal Thrust [N]	Duration of the thrust [s]	Area under curve [N.s]	Specific impulse [N.S/kg]	Regression rate [mm/s]
18,5	1,75	14,14	1208,97	X

Table 43: Thrust and specific impulse related values for PLA root_2 fuel grain.

Combusted grain weight [g]	Combusted oxidizer weight [g]	Pre-combustion dimension [mm]	After-combustion dimension [mm]
4,3	7,4	X	X

Table 44: Grain and oxidizer related values for PLA root_2 fuel grain.

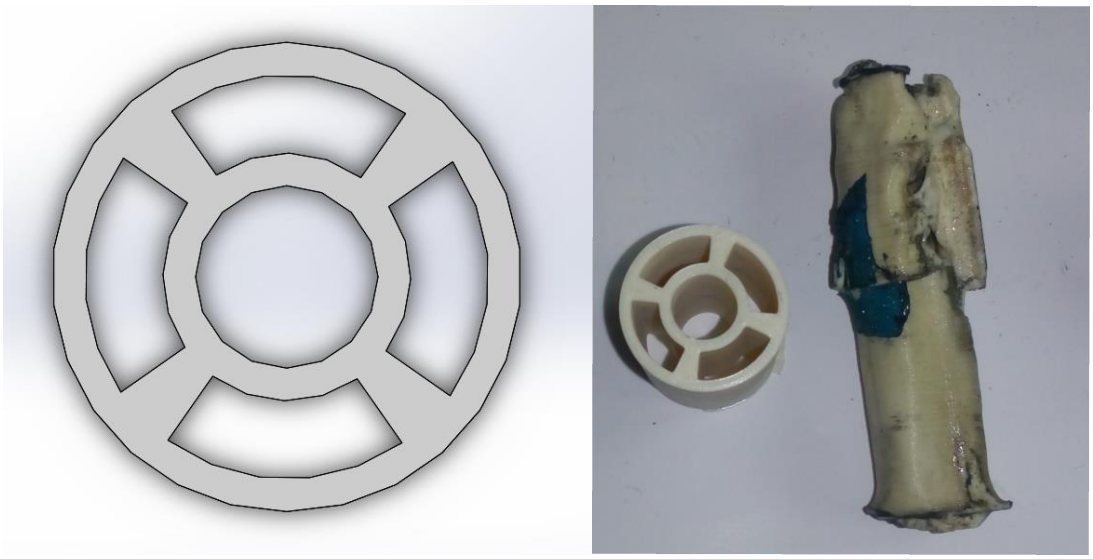

Fig. 26 Waggon wheel combustion port, beside central circular, here are 4 additional combustion sideports

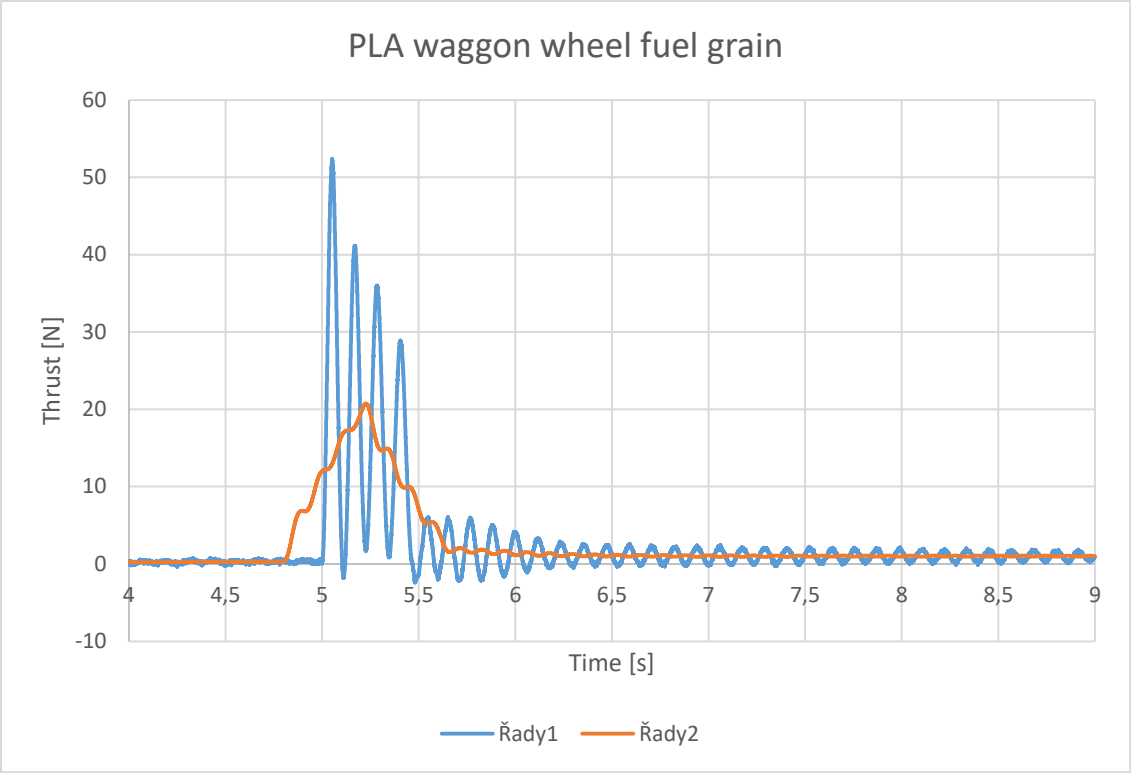

Chart 23: Thrust generated by PLA waggon wheel shaped fuel grain over time

Maximal Thrust [N]	Duration of the thrust [s]	Area under curve [N.s]	Specific impulse [N.S/kg]	Regression rate [mm/s]
20,75	0,87	9,28	977	X

Table 45: Thrust and specific impulse related values for PLA waggon wheel fuel grain.

Combusted grain weight [g]	Combusted oxidizer weight [g]	Pre-combustion dimension [mm]	After-combustion dimension [mm]
2,1	7,4	X	X

Table 46: Grain and oxidizer related values for PLA waggon wheel fuel grain.

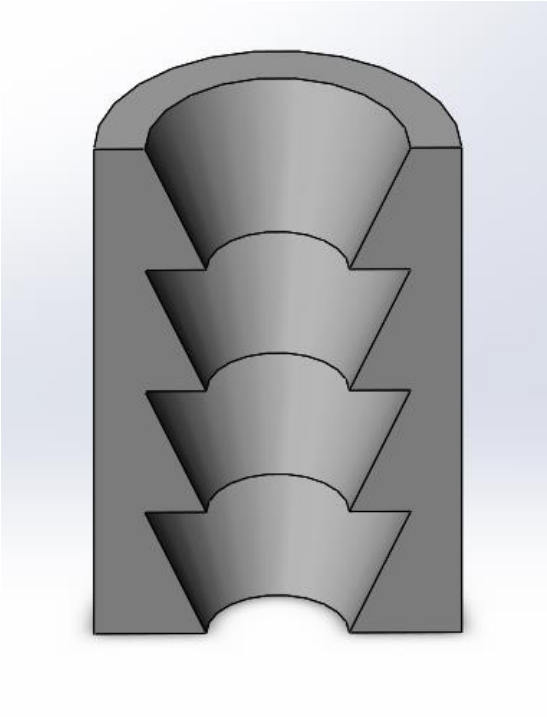

Fig. 27 Cross section along the length of grain, shoving internal "waves"

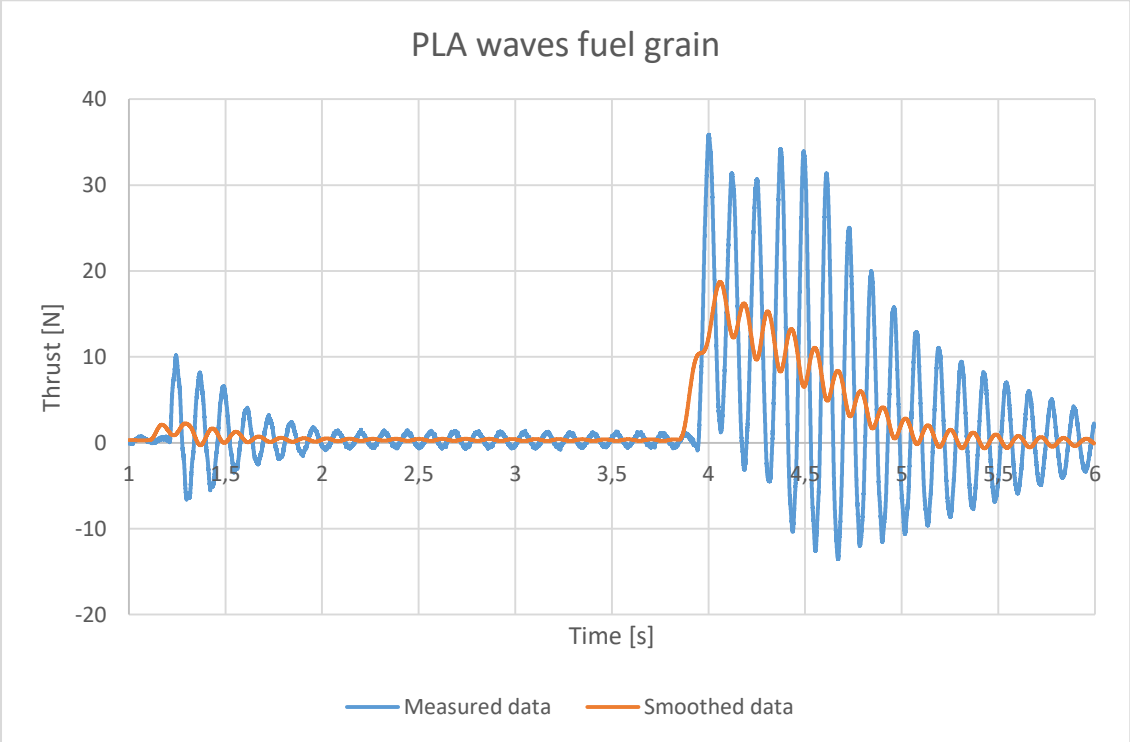

Chart 24: Thrust generated by PLA fuel grain with waves along the length of the combustion port over time

Maximal Thrust [N]	Duration of the thrust [s]	Area under curve [N.s]	Specific impulse [N.S/kg]	Regression rate [mm/s]
18,75	1,38	10,41	1095,91	1,29

Table 47: Thrust and specific impulse related values for PLA fuel grain with waves along the length of the combustion port fuel grain.

Combusted grain weight [g]	Combusted oxidizer weight [g]	Pre-combustion dimension [mm]	After-combustion dimension [mm]
2,1	7,4	7	8,78

Table 48: Grain and oxidizer related values for PLA fuel grain with waves along the length of the combustion port fuel grain.

	Cogwheel	Helix_2	Helix_4	Flower	Root_2	Waggon wheel	Waves
I_{sp}	1662,86	1199,27	1332,57	1289,8	1208,97	977	1095,91
Max. Thrust	23,5	24	18,5	16,5	18,5	20,75	18,75

Table 49: Summarized comparison of PLA prototype fuel grains

7. Conclusion

Based on the results of the measurements we can say that 3D printed fuel grains are definitely viable. In table 16, where we can see results of the tube shaped combustion ports from different materials and in which 3D printed tubes are compared to fuel grains supplied with the engine, can be clearly seen that both thrust and specific impulse produced by printed fuel grains is bested only by PVC and PP.

In following part we can see that combustion port shape influences the overall thrust and specific impulse. By employing more complex shapes of the combustion ports and increasing thus surface for the combustion maximal achieved thrust by PLA had increased compared to simple tube.

Even without engine being throttleable progress of thrust during time can be altered by using correct combustion port configuration. Unlike tube, some shapes can offer much more interesting progresses than rapid boost and slow regression after that. Shapes like root can offer two thrust peaks. Flower, star and circular main port with four helical side ports tend to maintain constant thrust for small amount of time.

3D printing of fuel grains is great tool for model rocketry and shows great promise for use in experiments. Fuel grain prototypes can be printed and used in smaller scale to find out, if the designed combustion port shape is suitable for desired application.

I_{sp}[N.s/kg]	Tube	Cross	Root	Star	Circular with side ports
PLA	1365,65	1401,58	1003,37	1852,21	1733,93
ABS	X	X	1298,59	701,24	1584,83
PET-G	1564,35	1289,8	2112,48	X	1464,78

Table 50: Summarized comparison of specific impulse produced by different combustion port shapes and grain materials

Thrust [N]	Tube	Cross	Root	Star	Circular with side ports
PLA	17,75	24,75	19	26	26
ABS	X	X	20,5	21	24,5
PET-G	18,5	16,5	22,9	X	22,5

Table 51: Summarized comparison of thrust produced by different combustion port shapes and grain materials

Nomenclature

Q = heat [J]

ρ = density [g/cm^3]

r = regression rate [mm/s]

Y = mass fraction

ΔH_f^O = heat of formation [J/kg]

T = temperature [K]

c_p = specific heat [J/g.K]

c_f= friction coefficient

G = average mass flux [m^3/s]

f_m = fuel/air mixing ratio

x = location along axis [mm]

D = diameter [mm]

$\Delta H_{v,eff}$ = total heat of glasification

C = coefficient, (approximately 0,03 for flow occurring in hybrid engine)

Re = Reynolds number

St = Stanton number

St_0 = Stanton number in the absence of blowing for turbulent flow over flat plate

u = velocity

h = enthalpy

R_1 = precombustion radius [mm]

R_2 = radius after combustion [mm]

t = time of the engine run [s]

r = regression rate [mm/s]

I_{sp} = specific impulse [N.s/kg]

A_{chart} = area under charted curvature [N.s]

m_b = mass burned during combustion (oxidizer and grain) [kg]

$m_{b,ox}$ = mass of burned oxidizer [kg]

$m_{b,gr}$ = mass of burned oxidizer [kg]

Subscipts:

e = edge of the boundary layer

fl = flame

w = wall

tot = total

f = fuel

ref = reference

s = surface

Abbreviations:

PLA = polylactic acid

ABS = acrylonitrile butadiene styrene

PET-G = polyethylene terephthalate glycol modified

CAD = computer aided design

O/F = oxidizer/fuel

LOX = liquid oxygen

PB = polybutadiene monomer

PBAN = polybutadiene monomer acrylonitrile

HTPB = hydroxyl-terminated polybutadiene monomer

CTPB = carbon terminated polybutadiene monomer

FLOX = fluorine and liquid oxygen mixture

FFF = fused filament fabrication

FDM = fused deposition modelling

CAM = computer aided manufacturing

SLA = stereolithography

SLS = selective laser sintering

DMLS = direct metal laser sintering

SLM = selective laser melting

CTU = Czech technical university in Prague

HDPE = high density polyethylene

PP = polypropylene

PVC = polyvinyl chloride

List of pictures:

List of literature:

[1] CHIAVERINI, Martin J a Kenneth K KUO. *Fundamentals of hybrid rocket combustion and propulsion*. Reston, Va.: American Institute of Aeronautics and Astronautics, c2007.

[2] FAVARÓ, F. M., W. A. SIRIGNANO, M. MANZONI a L. T. DELUCA. Solid-Fuel Regression Rate Modeling for Hybrid Rockets. *Journal of propulsion and power*. 2013, (Vol. 29, No. 1), 11. DOI: 10.2514/1.B34513.

[3] WALKER, Sean D. *High Regression Rate Hybrid Rocket Fuel Grains with Helical Port Structures*. Logan, Utah, 2015. Dissertation thesis. UTAH STATE UNIVERSITY.

[4] WHITMORE, Stephen A., Sean D. WALKER, Daniel P. MERKLEY a Mansour SOBBI. High Regression Rate Hybrid Rocket Fuel Grains with Helical Port Structures. *Journal of Propulsion and Power* [online]. 2015, **31**(6), 1727-1738 [cit. 2018-08-08]. DOI: 10.2514/1.B35615. ISSN 0748-4658. Dostupné z: http://arc.aiaa.org/doi/10.2514/1.B35615

[5] SUTTON, George P a Oscar BIBLARZ. *Rocket propulsion elements*. 8th ed. Hoboken, N.J.: Wiley, c2010. ISBN 978-0-470-08024-5.

[6] BATH, Andrew. *Performance Characterization of Complex Fuel Port Geometries for Hybrid Rocket Fuel Grains*. Logan, Utah, 2012. Master thesis. UTAH STATE UNIVERSITY.

[7] KLOSKI, Liza Wallach a Nick KLOSKI. *Getting started with 3D printing*. San Francisco: Maker media, 2016. ISBN 9781680450200.

[8] VAEZI, Mohammad, Hermann SEITZ a Shoufeng YANG. A review on 3D micro-additive manufacturing technologies. *The International Journal of Advanced Manufacturing Technology* [online]. 2013, **67**(5-8), 1721-1754 [cit. 2018-08-15]. DOI: 10.1007/s00170-012-4605-2. ISSN 0268-3768. Dostupné z: http://link.springer.com/10.1007/s00170-012-4605-2

[9] Bartel H. R., and Rannie,W. D., "Solid Fuel Combustion as Applied to Ramjets," Jet Propulsion Lab., Progress Rep. 3-12, California Inst. of Technology, Pasadena, CA, Sept. 1946.

[10] catmanEasy: Cz: *Hbm.cz* [online]. [cit. 2018-08-15]. Dostupné z: https://www.hbm.cz/produkty/software/catman-daq-software-sber-vyhodnoceni-dat/

En: *Hbm.cz* [online]. [cit. 2018-08-15]. Dostupné z: *Https://www.hbm.com/en/2290/catman-data-acquisition-software/*